

Simplicial cascades are orchestrated by the multidimensional geometry of neuronal complexes

Bengier Ülgen Kılıç^{1,*} and Dane Taylor^{1,†}

¹*Department of Mathematics, University at Buffalo, State University of New York, Buffalo, NY 14260, USA*

(Dated: January 7, 2022)

Wavefront propagation and the appearance of spatially distant clusters of activity generically arise in many contexts including neuron firing, social contagions, epidemics, and critical infrastructure failures. These phenomena are in direct competition and represent a frustration between the network's geometry and topology. Here, we extend their study to systems with higher-order interactions by analyzing cascades over *noisy geometric complexes*, which contain short- and long-range ‘simplices’ that encode dyadic, triadic, and high-order dependencies. We present a *simplicial threshold model* (STM) for cascades in which a vertex v_i becomes active only when the activity across its *simplicial neighbors*—including adjacent 1-simplices, 2-simplices, etc.—surpasses a threshold T_i . We show that higher-order interactions and thresholding can coordinate to robustly guide cascades along a geometric substrate comprised of lower-adjacent simplices despite the presence of long-range simplices. We explore this phenomenon for a simplicial-complex-based model of a neuronal network, i.e., a *neuronal complex*, revealing that higher-order interactions also promote the expressiveness and efficiency of diverse spatio-temporal patterns. We support these findings with bifurcation theory to predict wavefront and clustering dynamics as well as introduce *simplicial cascade maps* that embed simplicial complexes with a latent geometry in which pairwise distances reflect the time required for STM cascades to travel between vertices. Our findings and proposed mathematical tools reveal the dynamical/structural interplay of higher-order nonlinearity and the multidimensional geometry of simplicial complexes to be a fruitful direction for uncovering the multiscale mechanisms that orchestrate higher-order processing within complex systems.

* bengieru@buffalo.edu

† danet@buffalo.edu

I. INTRODUCTION

Cascading activity has been widely observed in diverse types of real-world systems including networks of spiking neurons [4, 57, 83], the dissemination of information and opinions across social networks [11, 15, 80, 90], epidemic spreading [28, 61, 72], failures within critical infrastructures [12, 13, 31], and traffic jams [55]. Models of such phenomena are often formulated as a spreading process in which a small, localized dynamical change produces an avalanching growth of effects across a network. Frequently, the network is spatially embedded [2] (i.e., neural circuitry within an organism or people/infrastructure dispersed across Earth’s surface) and there exist both short- and long-range edges [3, 91, 93], in which case cascades’ spatio-temporal patterns are determined by two competing phenomena [21, 22, 58, 60, 87]: *wavefront propagation (WFP)*, where spreading propagates locally across short-range edges; and the *appearance of new clusters (ANC)*, where it propagates to distant locations across long-range edges. Whether a cascade predominantly propagates locally versus globally informs experts on how to take appropriate steps toward analysis, prediction, control and/or sampling for various applications including advertisement-seeding strategies [5, 69], mitigation and containment of epidemics [27, 33, 44], neuromodulation and stimulation [41, 63], contingency analysis for power grids [31, 43], and management of supply chains [32, 59, 74].

However, WFP and ANC also depend on a cascade’s precise propagation mechanism. In social networks, for example, people are often reluctant to adopt a new belief/opinion unless several friends and family have already adopted it [20, 80], and such a threshold criterion causes social contagions to preferably spread locally via WFP, and ANC events occur less frequently [21, 22, 58, 87]. The integrate-and-fire mechanism of neurons is also a threshold criterion [49]; however, neurons exhibit a variety of other dynamical features (e.g., stochasticity, refractory periods, and inhibitory interactions [10]), thereby complicating the relation between thresholding and WFP/ANC. Importantly, recent research on neuronal cascades has illustrated how their spatio-temporal patterns’ diversity reflects a neuro-systems’ memory capacity [82], which helps explain certain cognitive impairments [56] and can be optimized by tuning the dynamics to criticality via a balancing of excitation/inhibition [4, 54]. Although local and nonlocal propagations have been experimentally studied (e.g., using spatial correlation analyses [78]) and modeled [75, 79] for neuronal networks, the mechanistic roles of WFP, ANC, and thresholding remain unclear regarding memory formation, neurocomputation, and higher-order cognitive processing.

At the same time, recent research has highlighted that dyadic (i.e., pairwise) interactions encoded in graphs are insufficient representations for many dynamical processes (e.g., circuit logic [46], neuron responses [23, 94], ecological networks [62], power-grid failures [37], supply chains [29], and group decision making [25, 52, 68, 73]), which has inspired rapid growth in developing models and theory for dynamical processes over hypergraphs and simplicial complexes that encode dyadic, tryadic, and higher-order combinatorial interactions. Simplicial-complex models have been employed to study the macroscopic activity of brain regions [6, 38, 76], and dynamical theory has been recently extended to many higher-order systems including synchronization models [16, 17, 36, 70], social contagions [30, 67], epidemic spreading [1, 7, 24, 42, 45, 86, 89], random walks and diffusion [18, 19, 34, 64, 71], consensus [65, 66, 81, 95], general models of ordinary differential equations [35, 53], and the optimization of higher-order dynamics [84, 96]. Nevertheless, it has not been explored how higher-order interactions affect cascades’ spatio-temporal WFP/ANC patterns nor the subsequent implications for neuro-computational systems.

Thus motivated, we extend a popular threshold model for cascades [40, 90] with binary dynamics [39] to develop theoretical insights for the combined effects of thresholding and higher-order interactions on nonlinear cascades over simplicial complexes. We propose a *simplicial threshold model (STM)* for cascades in which a vertex v_i becomes active only when the aggregate activity across its *simplicial neighbors*—which includes the states of adjacent edges, 2-simplices, and larger combinatorial sets of vertices—surpasses a threshold T_i . By assigning active/inactive states to vertices, edges, and higher-dimensional simplices, STM cascades provide a bridge between modeling frameworks that exclusively describe dynamics at the individual level (e.g., belief propagation and neuron firing) or at the group level (e.g., group decision making and the collective dynamics of cortical columns). It is natural to assume for some systems that groups influence individuals, and vice versa. However, such interactions are inherently difficult to represent by graphs, due to the different dimensionality of individuals and groups. STM cascades assign states to k -simplices of various dimension k , thereby allowing simplicial cascades to nonlinearly propagate in response to the states of individuals and of differently sized groups. Our model is intentionally simple to obtain concrete insights that may guide further investigation of simplicial cascades.

We study WFP and ANC phenomena for STM cascades over *noisy geometric complexes* that contain both short- and long-range simplices. Short-range simplices provide a “substrate” structure that contains k -dimensional geometrically reinforced channels for cascades to locally follow via WFP. In contrast, long-range simplices impose a topological perturbation, or ‘noise’, to the geometrical substrate. As shown in Fig. 1, the nonlinear interplay between higher-order interactions, thresholding, and the presence of short- and long-range simplices has complicated effects on the spatio-temporal patterns of STM cascades. We find that thresholding and higher-order interactions play a similar mechanistic function: they both inhibit long-range spreading, which leads to less frequent ANC and promotes local WFP. Moreover, their combination more robustly guides STM cascades along the geometrical substrate, thereby enabling cascades to reliably spread by WFP despite the presence of topological noise.

This mechanism for robustly organizing the spatio-temporal patterns of higher-order cascades has significant implications for the aforementioned applications in which dyadic-interaction models insufficiently represent cascades. As a concrete example, we develop computational experiments to study STM cascades over a simplicial complex model for a *C. Elegans* neuro-system

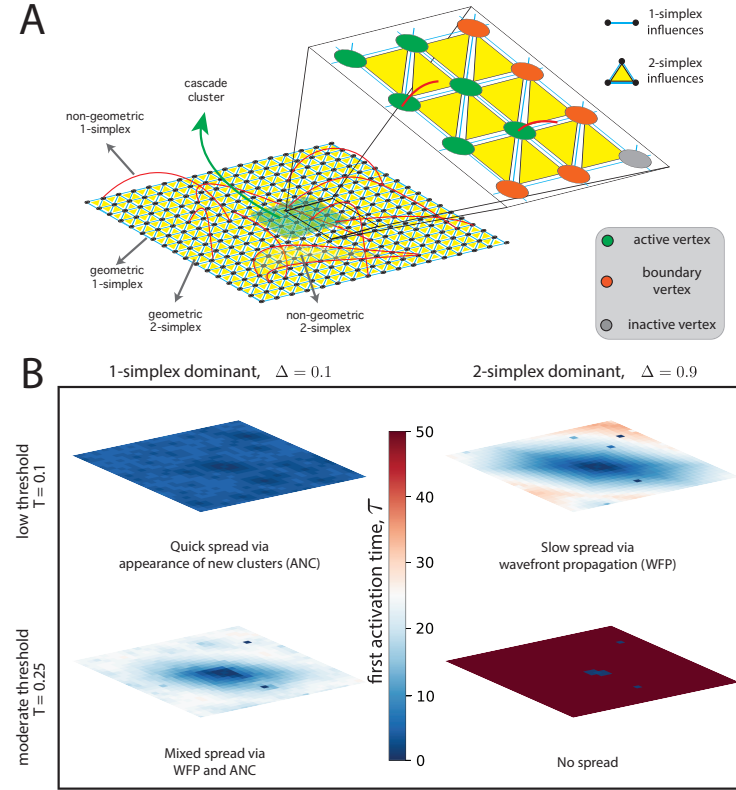


FIG. 1. Local and nonlocal spreading patterns for a simplicial threshold model (STM) for cascades on a 2-dimensional (2D) noisy geometric complex. (A) A STM cascades is initialized near the center of a clique complex that is associated with a spatial graph in which vertices are arranged in a 30×30 triangular lattice. Vertices have $d^{(G)} = 6$ short-range *geometric edges* to nearest neighbors (although vertices on the outside have fewer) and $d^{(NG)} = 1$ long-range *non-geometric edge* (which are added uniformly at random between pairs of vertices). A STM cascade can propagate locally over geometric simplices in the form of wavefront propagation (WFP) or non-locally over non-geometric simplices to cause the appearance of new clusters (ANC). Propagation to a *boundary vertex* v_i requires the aggregate activity across its simplicial neighbors—which includes adjacent 1-simplices, 2-simplices, etc.—to surpass a threshold T . Here, we study 2D STM cascades in which the relative interaction strength of 2-simplices versus 1-simplices is tuned by a parameter $\Delta \in [0, 1]$ (see Eq. 2). (B) Cascades' spatio-temporal patterns express a frustration between WFP and ANC, which we visualize for different T and Δ by showing for each vertex v_i the time τ_i at which it first becomes active. When T and Δ are both small, simplicial cascades rapidly progress via ANC. Increasing either T or Δ suppresses ANC, although increasing Δ does this more effectively. Cascade won't spread if T and/or Δ are too large.

[48, 92]. In this example, we represent experimentally observed neuronal synapses by edges in a graph, and we represent higher-order nonlinear dependencies between neurons [77] in an associated simplicial complex, which we refer to as a *neuronal complex*. Our experiments reveal that higher-order interactions increase the expressiveness, or diversity, of neuronal cascades, which is a hallmark of enhanced memory capacity [82]. Thus, higher-order interactions may play a crucial role in determining both the pathways/channels over which neuronal cascades propagate and the extent to which distinct stimuli lead to distinct cascade-pattern responses. Moreover, we show that higher-order interactions also improve the efficiency of cascades—that is, they allow for diverse patterns to arise for smaller threshold values, which implies that less energy is required per neuron activation.

We support these findings with bifurcation theory to predict WFP speeds and the rates of ANC events for STM cascades over k -dimensional channels. Our theory relies on a combinatorial analysis that considers the various possible responses for *boundary vertices*, which have active neighbors but themselves are not yet active. We also introduce *simplicial cascade maps* that attribute simplicial complexes with a latent geometry in which pairwise distances reflect the time required for STM cascades to travel between vertices. Simplicial cascade maps are a simplicial-complex generalization of contagion maps [87], and they may similarly be used to quantitatively study the competition between WFP and ANC using techniques from high-dimensional data analysis, nonlinear-dimension reduction, manifold learning, and topological data analysis. Our proposed mathematical tools and computational experiments reveal that the multidimensional geometry of simplicial complexes can coordinate with the nonlinear propagation mechanism of thresholding to robustly organize higher-order cascades, which is a promising direction for uncovering the multiscale mechanisms responsible for higher-order processing in neuro-systems, and more broadly, the spatio-temporal patterns of higher-order cascades across other social, biological, and technological systems.

II. RESULTS

A. Simplicial threshold model (STM) for cascades

We begin by defining STM cascades, which requires some description of notation for simplicial complexes. Let $G(\{\mathcal{C}_k\}_{k=0}^K)$ be an K -dimensional simplicial complex with sets \mathcal{C}_k that contain the simplices of dimension k . For example, a 1-dimensional (1D) simplicial complex is a graph $G(\{\mathcal{C}_k\}_{k=0}^1)$, \mathcal{C}_0 is a set of vertices, and \mathcal{C}_1 is a set of undirected, unweighted edges. Each vertex $v_i \in \mathcal{C}_0$ is assigned a coordinate $\mathbf{y}^{(i)} \in \mathbb{R}^p$ in a p -dimensional *ambient* metric space. (Note that vertices in “abstract” simplicial complexes do not have such coordinates.) We assume a Euclidean metric, although it may be advantageous to explore other metric spaces [8, 51]. For each vertex $v_i \in \mathcal{C}_0$, we define d_i^k as the number of k -simplices to which it is adjacent: d_i^1 is the *1-simplex degree* of vertex v_i (often called node degree for graphs), d_i^2 is its *2-simplex degree*, and so on. We also define for each vertex v_i the sets $\mathcal{N}^k(i) = \{s \in \mathcal{C}_k | i \in s\}$ that contain its k -dimensional *simplicial neighbors*. It follows that $d_i^k = |\mathcal{N}^k(i)|$ for each vertex v_i and simplex dimension k .

We now define STM cascades in which all k -simplices of dimension $k \leq \kappa$ are given binary dynamical states $x_i^k(t) \in \{0, 1\}$, i.e., *inactive* vs *active*, where index i enumerates the simplices of dimension k and $t \geq 0$ is time. For 2-dimensional (2D) STM cascades (i.e., $\kappa = 2$), the states of vertices, 1-simplices, and 2-simplices are given by $\{x_i^0(t)\}$, $\{x_i^1(t)\}$, and $\{x_i^2(t)\}$, respectively. Parameter κ is called the *STM cascade’s dimension*, and it may differ from that of the simplicial complex as long as $\kappa \leq K$. For $k > 0$, the states of k -simplices are directly determined by the states of vertices; a k -simplex (v_1, \dots, v_{k+1}) is active only when k of the vertices are active. For example, an edge (v_i, v_j) is active if at least one vertex v_i or v_j is active, and a 2-simplex is active if at least two of the three vertices are active. When vertices change their states, we allow k -simplices with $k > 0$ to update their states instantaneously, and we leave open the investigation of more complicated dependencies such as delayed state changes for higher-dimensional k -simplices and other rules for how their states depend on those of vertices and possibly other k -simplices. In Fig. 2(A), we visualize the states of vertices, 1-simplices, and 2-simplices. We present examples from the perspective of a *boundary vertex*, which we define as a vertex that is inactive but has at least one active simplicial neighbor.

The vertices’ states evolve via a discrete-time process that we define in Methods Section ‘STM cascades’. Here, we present a simplified dynamics for 2D STM cascades. At time step $t + 1$, the state $x_i^0(t)$ of each vertex v_i possibly changes according to a threshold criterion

$$x_i^0(t+1) = \begin{cases} 1, & \text{if either } x_i^0(t) = 1 \text{ or } R_i(t) > T_i, \\ 0, & \text{if } x_i^0(t) = 0 \text{ and } R_i(t) \leq T_i, \end{cases} \quad (1)$$

where T_i is an *activation threshold* intrinsic to vertex v_i and

$$R_i(t) = (1 - \Delta) f_i^1(t) + \Delta f_i^2(t) \quad (2)$$

is a weighted average of cascade activity across the simplicial neighbors of vertex v_i .

Parameter Δ tunes the relative influence of 2-simplices and $f_i^1(t) = \frac{1}{d_i^1} \sum_{j \in \mathcal{N}_A^1(i, t)} x_j^1(t)$ and $f_i^2(t) = \frac{1}{d_i^2} \sum_{j \in \mathcal{N}_A^2(i, t)} x_j^2(t)$ are the fraction of 1-simplices and 2-simplices adjacent to vertex v_i that are active at time t . One can also interpret $R_i(t)$ as v_i ’s “simplicial exposure” to the cascade at time t . Notably, the limit $\Delta \rightarrow 0$ yields a 1-dimensional (1D) STM cascade, which recovers the Watts threshold model [90] for cascades over graphs.

To narrow the scope of our computational experiments, herein we initialize all STM cascades at time $t = 0$ using *cluster seeding* (see Methods Section ‘Cluster seeding’), in which case we select a vertex, and set all of its adjacent vertices to be active, while all other vertices are inactive. Thresholding can potentially prevent localized initial conditions from propagating into large-scale cascades [40, 87], and cluster seeding helps overcome this dynamical barrier. Finally, our experiments are also simplified by assuming identical thresholds for each vertex, $T_i = T, \forall i \in \mathcal{C}_0$. This allows us to explore the cooperative effects of thresholding and higher-order interactions by varying only two parameters: threshold T and 2-simplex influence Δ .

B. STM cascades over noisy geometric complexes

We study the spatio-temporal patterns of STM cascades over *noisy geometric complexes*, which contain both short- and long-range simplices and are a generalization of noisy geometric networks [87]. Short- and long-range interactions have been observed in a wide variety of applications (e.g., face-to-face and online interactions in social networks) and are known to play an important structural/dynamical role for neuronal activity [75, 79]. It’s also worth noting that noisy geometric networks exhibit the small-world property [91] under certain parameter choices, and noisy geometric complexes will likely exhibit a simplicial analogue to this property [9, 50].

We assume that the vertices \mathcal{C}_0 lie along a manifold within an ambient space \mathbb{R}^p , and that all k -simplices are one of two types:

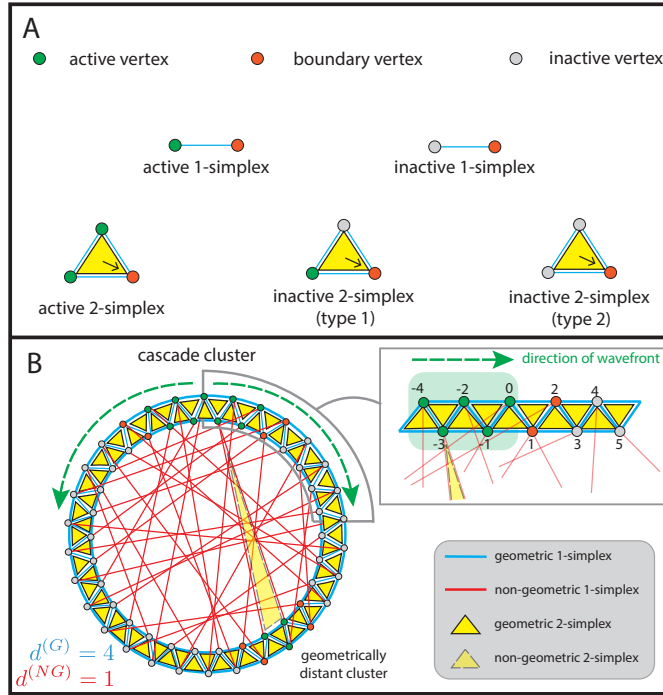


FIG. 2. **Wavefront propagation for STM Cascades along Noisy Ring Complexes.** (A) Each k -simplex has a binary state $x_i^k(t) \in \{0, 1\}$ indicating whether it is inactive or active, respectively, at time t . Active k -simplices influence inactive boundary vertices, possibly causing them to become active at the next time step. The dimension κ of an STM cascade refers to the highest-dimension k -simplex that is utilized, and we focus herein on 2D STM cascades. (B) Noisy ring complexes generalize noisy ring lattices [87] and involve vertices that lie along a 1D manifold, which is embedded in a 2D ‘ambient’ space. (Vertices are visualized alongside the manifold here to allow easy visualization of 2-simplices.) In this example, each vertex has $d^{(G)} = 4$ geometric edges to nearby vertices and $d^{(NG)} = 1$ nongeometric edge to a distant vertex. Higher-dimensional simplices arise in the associated clique complex and are similarly classified. An STM cascade exhibits WFP when it propagates along the manifold via geometric simplices, and ANC events when it jumps across a non-geometric simplex.

geometric simplices that connect vertices that are nearby on the manifold, and long-range *non-geometric simplices* that connect distant vertices. Each k -simplex is considered to be geometric if and only if all of its associated edges are geometric. After categorizing k -simplices as geometric or non-geometric, we further refine the notion of k -simplex degrees. Specifically, we let $d_i^{k,G}$ and $d_i^{k,NG}$ denote *geometric* and *non-geometric* k -simplex degrees, respectively, of a vertex v_i so that $d_i^k = d_i^{k,G} + d_i^{k,NG}$.

In Fig. 1, we depict a noisy geometric complex embedded on a 2D plane, whereas we depict one embedded on a 1D ring manifold in Fig. 2. In our synthetic models, we construct geometric edges by connecting each vertex to several of its nearest neighbors. In contrast, we create non-geometric edges uniformly at random between pairs of vertices that do not yet have an edge. In either case, we construct noisy geometric complexes by considering the associated clique complexes for these vertices and edges. See Methods Section ‘Generative model for noisy ring complexes’ for further details about this construction.

Before continuing, we highlight that it is important to understand the different types of ‘dimension’ that have been introduced. The dimension K of a simplicial complex refers to the maximum dimension of its k -simplices. For a noisy geometric complex, we assume it lies on a low-dimensional manifold within a p -dimensional metric space. Finally a STM cascade has its own dimension, κ , which is the largest k -simplex dimension that is utilized by the nonlinear dynamics. All of these dimensions can differ, and the only required relation is that the manifold dimension is less than or equal to p .

C. Simplicial cascades robustly follow geometrical channels

Thresholding and higher-order interactions both suppress non-local ANC across non-geometric edges, which promotes simplicial cascades to locally propagate via WFP along geometric edges. This is supported in Fig. 1, where we study 2D STM cascades over a 2D noisy geometric complex. (The manifold, simplicial complex, and STM cascades coincidentally all have the same dimension in this example.) We initialized STM cascades with cluster seeding at a central vertex so that it could potentially spread outward via WFP along the 2D manifold.

In Fig. 1(B), we visualize the *activation times* τ_i (i.e., when each vertex v_i first becomes active), showing results for STM cascades with four choices for the parameters T and Δ . Observe for small T and Δ (top-left subpanel) that STM cascades rapidly

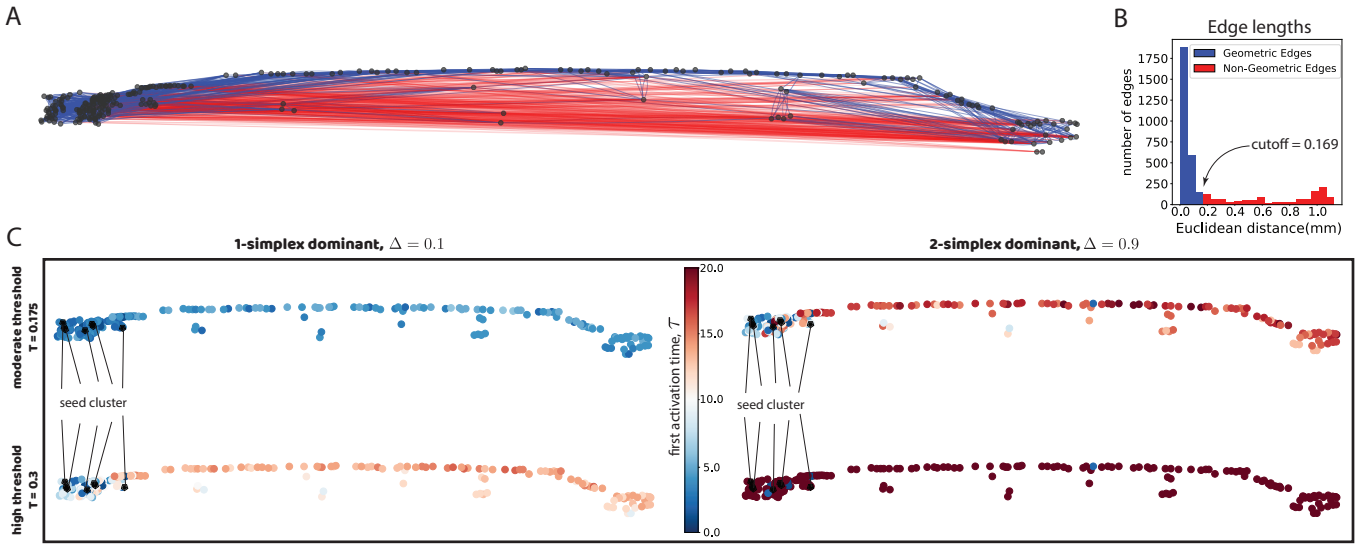


FIG. 3. STM cascades on a *C. Elegans* neuronal complex. (A) 2D visualization of experimentally measured locations and synapse connections between neurons in nematode *C. Elegans* [48, 92]. k -simplices in the associated clique complex represent higher-order nonlinear dynamical dependencies among sets of $(k + 1)$ neurons for different k . (B) We consider a histogram of edge lengths and choose a cutoff distance of 0.169 mm to distinguish geometric and non-geometric simplices. (C) Vertices' colors depict their first-activation times τ_i for a 2D STM cascade that is initialized with the indicated seed cluster. Observe that T and Δ affect WFP and ANC similarly to what was shown in Fig. 1(B).

spread and predominantly exhibit ANC, which results in the ‘splotchy’ pattern. In contrast, when either T or Δ is increased, the simplicial cascade predominantly exhibits WFP, and not ANC, which slows propagation and enables the cascade to more reliably follow along the geometric substrate. (i.e., thereby overcoming the presence of long-range topological ‘noise’). Finally, observe that if T and Δ are too large (bottom-right subpanel), then the initial seed cluster does not lead to a cascade.

This finding extends existing knowledge about the effects of short- and long-range connections on cascades. It is well-known that long-range edges allow traditional pairwise-progressing cascades to rapidly spread via the mechanism of ANC. This concept is most apparent in the context of epidemic spreading, and as a response, banning international airline travel is often a first response to prevent long-range transmissions for epidemics [27, 33, 44]. However, ANC is also diminished when the cascade’s propagation mechanism requires a vertex’s neighboring activity (i.e., ‘exposure’) to surpass a threshold T [20–22, 58, 87]. We find that higher-order interactions can be as, if not more, effective at suppressing nonlocal ANC. Moreover, these two mechanisms can coordinate to more robustly guide cascades along a geometrical substrate, or channel, despite the presence of topological (i.e., non-geometric) noise.

D. STM cascades on a *C. Elegans* neuronal complex

We observe similar cooperative effects of thresholding and higher-order interactions for STM cascades on a *neuronal complex*, which we define as a simplicial complex model that represents the higher-order nonlinear interdependencies between neurons. We study simplicial cascades over a neuronal complex representation for the neural circuitry and dynamics for nematode *C. Elegans* [48, 92]. In this example, vertices represent neurons’ somas (i.e., cell bodies), edges represent experimentally observed synapses, and higher-order simplices encode potential higher-order nonlinear dynamical relationships between combinatorial sets of neurons [77], which we encode here using clique complexes.

In Fig. 3(A), we visualize the *C. Elegans* neuronal complex. The locations of vertices reflect experimental measurements for the somas’ centers. The length of each edge denotes the distance between somas, which we use as an estimate for the combined lengths of the axon and dendrite involved in each synapse. Geometric and non-geometric edges are indicated by blue and red lines, respectively. For simplicity, we do not visualize higher-dimensional simplices. We provide a histogram of edge lengths in Fig. 3(B), and observe that most edges are short-range, but there are also many long-range connections. We heuristically classify edges as geometric/non-geometric depending on whether edge lengths are less than or greater than a “cutoff” distance of 0.169 mm. Note that this choice of threshold has no effect on the dynamics of STM cascades. Finally, we construct a neuronal complex by considering the graph’s associated clique complex.

Observe that the *C. Elegans* neuronal complex largely lies along a 1D manifold that is embedded 2D, which occurs due to the elongated shape of a nematode worm. Thus, we are interested in understanding the extent to which simplicial cascades

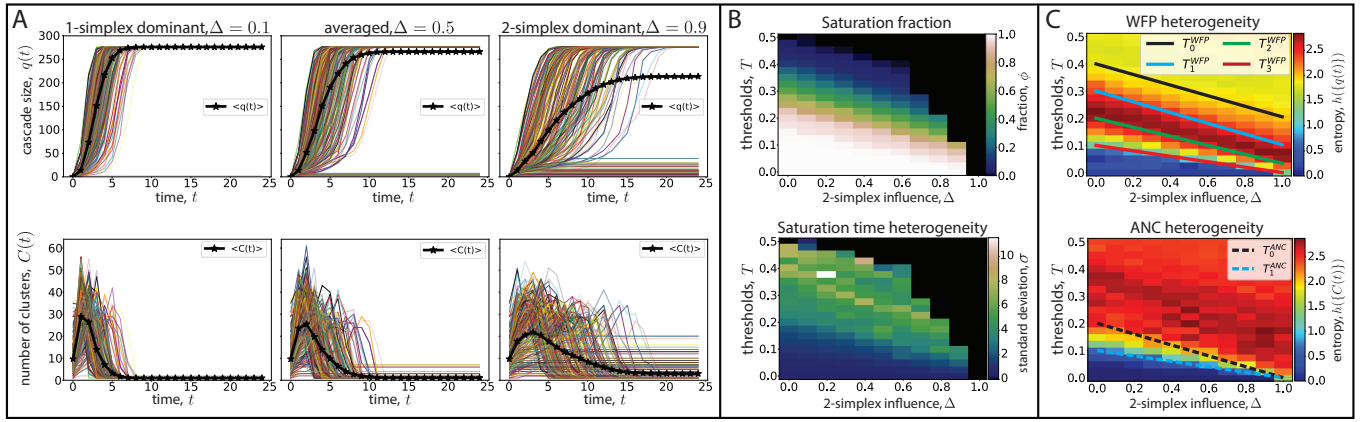


FIG. 4. Higher-order interactions promote pattern expressiveness and efficiency for STM cascades on a *C. Elegans* neuronal complex. **(A)** Cascade size $q(t)$ (top) and the number $C(t)$ of spatially disjoint clusters (bottom) versus time t for 2D STM cascades with threshold $T = 0.1$ and $\Delta \in \{0.1, 0.5, 0.9\}$. Different curves represent different initial conditions, and black curves give their means. **(B)** For STM cascades with different T and Δ , colors indicate (top) the fraction ϕ of initial conditions in which a cascade ‘saturates’ the neuronal complex (i.e., spreads everywhere) and (bottom) the standard deviation σ of the times at which saturations occur. Black regions indicate (T, Δ) values for which no cascades saturate the network. Cascades are most heterogeneous when T and Δ are neither too small or large. **(C)** Colors indicate the heterogeneity of WFP and ANC properties by showing (top) $h(\{q(t)\})$ and (bottom) $h(\{C(t)\})$, where $h(\cdot)$ denotes the discrete Shannon entropy of a set of cascades with different initial conditions (see Methods Section ‘Entropy Calculation’). We focus on time $t = 5$, since these measures are most reflective of WFP and ANC at early times. Lines indicate bifurcation theory that we describe in the ‘Bifurcation theory for STM Cascades over 1D geometrical channels’ section. Observe that increasing Δ causes the dynamical changes to occur for smaller T , which lowers the energy consumption per neuron activation.

locally propagate by WFP along the 1D manifold versus nonlocal ANC events. To provide insight, in Fig. 3(C) we visualize first activation times τ_i for 2D STM cascades with different parameters T and Δ . These subpanels recapitulate our findings for the 2D case that were shown in Fig. 1(B): thresholding and higher-order interactions suppress nonlocal ANC and can cooperatively promote WFP along a geometric substrate or channel.

While our knowledge of neuronal cascades has grown immensely in recent years [4, 54, 57, 82, 83] the mathematical mechanisms responsible for directing how and where cascades propagate have remained elusive. The coordination of higher-order nonlinear thresholding and the multidimensional geometry of simplicial complexes is a plausible structural/dynamical mechanism that can help self-organize neuronal cascades. In brains, for example, thresholding and higher-order interactions can potentially be modulated in real time using neuro-transmitters and synaptic plasticity to help direct cascades. Of course, the combined effects of other dynamical features (e.g., refractory periods, inhibition, and stochasticity) should also be explored. Nevertheless, our work highlights this emerging field as a promising direction for unveiling the multiscale mechanisms that orchestrate higher-order information processing within complex cognitive systems, including biological, social and technological systems.

E. Simplicial cascades enhance pattern expressiveness and efficiency

Higher-order interactions promote heterogeneity for STM cascades’ spatio-temporal patterns, which has important implications in the context of neuronal cascades. Specifically, neuronal networks that exhibit more ‘expressive’ activity patterns have broader memory capacity [82, 83], which has been shown to occur for neuronal networks that are tuned near ‘criticality’—i.e., a dynamical phase transition. At the same time, there is extensive empirical evidence that neuron interactions are higher-order [77, 94], yet mathematical theory development for neuronal cascades has largely remained limited to dyadic-interaction models (see, e.g., [54]).

In Fig. 4, we study how parameters T and Δ effect the heterogeneity of STM cascades on the *C. Elegans* neuronal complex. In Fig. 4(A), we study WFP (top) and ANC (bottom) properties by plotting the cascade size $q(t)$ and the number of clusters $C(t)$, respectively, as STM cascades propagate. The left, center, and right columns show results for STM cascades that are 1-simplex dominant ($\Delta = 0.1$), averaged ($\Delta = 0.5$) and 2-simplex dominant ($\Delta = 0.9$), respectively. In each subpanel, different curves represent different initial conditions, whereby we select different vertices to initiate cluster seeding. Black curves indicate the means across initial conditions. Observe that some STM cascades spread to the entire neuronal complex and are said to *saturate* the network, whereas others do not. Also, early on, the numbers of clusters increase due to ANC, but these numbers can later decrease as clusters grow and merge. Moreover, there is significant heterogeneity across the different cascades’ initializations,

which arise due to the heterogeneous connectivity of neurons within the neuronal complex. This heterogeneity becomes more prominent as Δ (the 2-simplex influence) increases.

In Fig. 4(B), we further study cascade heterogeneity for different initial conditions and different choices for T and Δ . We plot (top) the fraction ϕ of cascades that saturate the network and (bottom) the standard deviation σ for the times at which saturations occur. The black-colored regions highlight that no STM cascades saturate the network if T and/or Δ are too large. Observe that the cascades' saturation fractions and times are most heterogeneous when T and Δ are neither too small or too large. This suggests thresholding and higher-order interactions may also play a 'critical' role for tuning neuronal networks to exhibit heightened cascade pattern diversity (which is called 'wide dynamic range' when considered from a multiscale perspective).

In Fig. 4(C), we focus on $q(t)$ and $C(t)$ when $t = 5$, which is an early time in which these values provide empirical quantitative measures for WFP and ANC, respectively. (At larger times t , it is difficult to distinguish WFP and ANC propagations since the cascades are so large.) For different T and Δ , we study the heterogeneity of these values by computing the Shannon entropy of (top) $h(\{q(t)\})$ and (bottom) $h(\{C(t)\})$ across the different initial conditions. See Methods Section 'Entropy Calculation' for details. Observe that the entropy of cascade sizes is largest when T and Δ are neither too small or too large, which is similar to our finding in Fig. 4(B). When considering $h(\{C(t)\})$, we do not observe a similar peak for intermediate values of T and Δ ; however the changes in entropy for $C(t)$ and $q(t)$ occur at approximately the same values of T and Δ , since the dynamics (i.e., ANC and WFP phenomena) undergo changes at these particular parameter choices.

By considering STM cascades across the (T, Δ) parameter space, we can systematically investigate the complementary effects of thresholding and higher-order interactions. We will develop bifurcation theory in the next section to guide this exploration, which is represented by the solid and dashed lines in Fig. 4(C). Before continuing, we highlight in Figs. 4(B) and 4(C) that as Δ increases, the dynamical changes can be observed to occur at smaller values of T . This has important implications for the efficiency of neuronal systems. When the threshold T is smaller, it requires fewer neighboring activations to induce a neuron to activate. Thus, small-threshold systems inherently consume less energy, per activation. Since larger Δ allows for heterogeneous cascade patterns to arise for smaller T , this suggests that higher-order interactions can also enhance the efficiency of neuronal activity.

F. Bifurcation theory for STM Cascades over 1D geometrical channels

We analyze WFP and ANC for STM cascades over a family of simplicial complexes in which N vertices lie along a 1D manifold as shown in Fig. 2(B). See Methods Section 'Generative model for noisy ring complexes' for their formation, which generalizes the noisy ring lattices that are studied in [87], wherein the authors developed bifurcation theory to predict WFP and ANC properties for a threshold-based cascade model that is restricted to dyadic interactions. In the Methods Section 'Combinatorial analysis for bifurcation theory' we describe bifurcation theory that characterizes STM cascades over noisy ring complexes. Our theory assumes large N and is based on a combinatorial analysis for the different possible state changes for boundary vertices that have active simplicial neighbors, but they themselves are not yet active. We focus on the early stage of cascades in which they are just beginning to spread, and we summarize our results below.

Our primary findings are two sequences of critical thresholds that characterize WFP and ANC and which depend on the STM parameter Δ and degrees $d^{(G)}$, $d^{(NG)}$, d_i^1 , and d_i^2 . The qualitative properties of WFP are determined by critical thresholds

$$T_j^{WFP} = (1 - \Delta) \frac{s_j}{d_i^1} + \Delta \frac{1}{d_i^2} \binom{s_j}{2}, \quad (3)$$

where $s_j = d^{(G)}/2 - j$ and $j \in \{0, 1, \dots, d^{(G)}/2\}$. The first and second terms in Eq. (3) represent 1-simplex and 2-simplex influences, respectively. While the thresholds T_j^{WFP} may differ for vertices v_i that have different k -simplex degrees, they are the same for simplicial complexes that are " k -simplex degree-regular". Unless otherwise noted, in our experiments we focus on thresholds associated with the median k -simplex degrees. The resulting critical thresholds identify ranges $T \in [T_{j+1}^{WFP}, T_j^{WFP})$ such that the speed of WFP properties are identical for any threshold T within a given range. Within each range, the WFP speed is $2j + 2$. There is no WFP when $T > T_0^{WFP}$. Similarly, the qualitative properties of ANC are determined by critical thresholds

$$T_j^{ANC} = (1 - \Delta) \frac{d^{(NG)} - j}{d_i^1}, \quad (4)$$

where $j \in \{0, 1, \dots, d^{(NG)}\}$. An ANC event involves a nonlocal boundary vertex v_i becoming active, which require a certain level of activity across its nongeometric simplicial neighbors (i.e., adjacent 1-simplices and 2-simplices that are long-range). The probability of that happening is the same for any $T \in [T_{j+1}^{ANC}, T_j^{ANC})$, and it is different for any two T values in different regions. Notably, there is no ANC if $T > T_0^{ANC}$. Note there is not a second term in the right-hand side of Eq. 4, which occurs because non-geometric 2-simplices extremely rarely occur in the limit of large N , since non-geometric edges are added uniformly at random to a noisy ring complex.

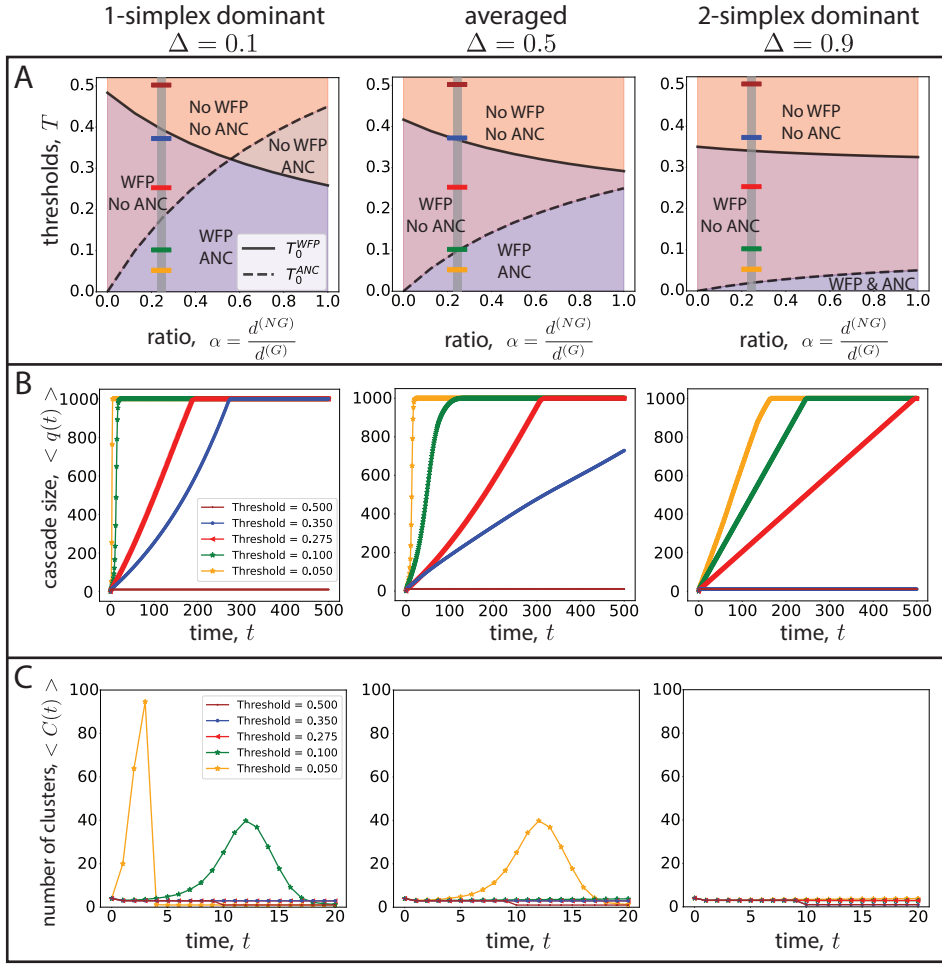


FIG. 5. Bifurcation theory predicts WFP and ANC behaviors on 1D manifolds. We consider 2D STM cascades over noisy ring complex (recall Fig. 2) for various T and either (left) $\Delta = 0.1$, (center) $\Delta = 0.5$, or (right) $\Delta = 0.9$. (A) Bifurcation diagrams depict the critical thresholds T_0^{WFP} and T_0^{ANC} given by Eqs. (3) and (4), respectively, for the (α, T) parameter space, which reveals four regimes that are characterized by the absence/presence of WFP and ANC. Observe that increasing Δ inhibits ANC, and in fact, the regime of ANC with no WFP entirely vanishes for $\Delta > 0.1$. Vertical gray lines and horizontal colored lines indicate the values $\alpha = 0.25$ and $T \in \{0.05, 0.1, 0.275, 0.35, 0.5\}$, for which STM cascades are further studied in panels (B) and (C). (B) Colored curves indicate the sizes $q(t)$ of STM cascades versus time t , averaged across all possible initial conditions with cluster seeding. (C) Colored curves indicate the average number of clusters $C(t)$, and one can observe a peak only when ANC occurs. Three scenarios give rise to WFP and ANC: $(\Delta, T) \in \{(0.1, 0.05), (0.1, 0.1), (0.5, 0.05)\}$. Four scenarios give rise to no spreading: $(\Delta, T) \in \{(0.1, 0.5), (0.5, 0.5), (0.9, 0.35), (0.9, 0.5)\}$. The other selected values of Δ and T yield WFP and no ANC, in which case $q(t)$ grows linearly.

In Fig. 5(A), we show bifurcation diagrams that characterize the absence/presence of WFP and ANC properties for different choices of T and the ratio $\alpha = d^{(NG)}/d^{(G)}$. Solid and dashed black curves indicate T_0^{WFP} and T_0^{ANC} , respectively. Different columns depict bifurcation diagrams for different STM cascades that are either: (left, $\Delta = 0.1$) 1-simplex dominant; (center, $\Delta = 0.5$) averaged; or (right, $\Delta = 0.9$) 2-simplex dominant. The vertical gray lines and horizontal colored lines indicate choices for α and T that are further studied in Figs. 5(B) and 5(C). Observe in Fig. 5(A) that as Δ increases, the region of parameter space exhibiting WFP and no ANC expands, whereas the region exhibiting WFP and ANC shrinks. Notably, the region exhibiting ANC and no WFP vanishes altogether for $\Delta > 0.1$. In other word, as STM cascades are more strongly influenced by higher-order interactions, they exhibit an increase in WFP and a decrease in ANC. The cascades more robustly propagate via WFP along the geometric channel/substrate, and they are less impacted by the ‘topological noise’ that is manifest as long-range, non-geometric simplices.

In Figs. 5(B) and 5(C), we plot cascade size $q(t)$ and number of clusters $C(t)$, respectively, which are averaged across all initial conditions for cluster seeding, as a function time t . As before, the left, center and right columns depict the choices $\Delta \in \{0.1, 0.5, 0.9\}$. In each panel, we show several curves for different thresholds $T \in \{0.05, 0.1, 0.275, 0.37, 0.5\}$. All panels reflect results for noisy ring complexes with $d^{(G)} = 8$ and $d^{(NG)} = 2$, so that $\alpha = 0.25$. Our selection for these choices of α and

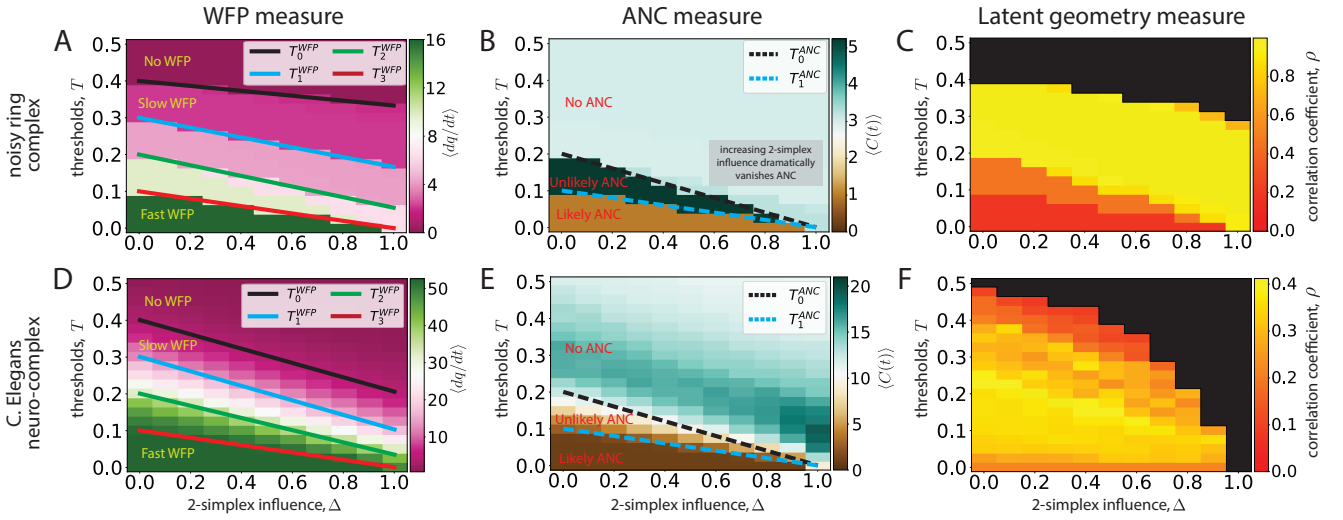


FIG. 6. **Empirical measurements for WFP and ANC rates predicted by critical thresholds T_j^{WFP} and T_j^{ANC} .** We study 2D STM cascades with various T and Δ over (top row) a noisy ring complex with $N = 1000$ vertices, $d^{(G)} = 8$, and $d^{(NG)} = 2$ and (bottom row) the C. Elegans neuronal complex. (A) An empirical measure for WFP speed, $\frac{dq}{dt}$, which we compute at $t = 5$ and average across all initial conditions with cluster seeding. Observe that $\frac{dq}{dt}$ undergoes changes at the critical thresholds T_j^{WFP} given by Eq. (3), which vary with Δ . Within each region $T \in [T_{j+1}^{WFP}, T_j^{WFP}]$, observe that the growth rate is close to our predicted rate of $2j + 2$. (B) An empirical measure for ANC, $C(t)$, which we compute at $t = 5$ and average across initial conditions. Observe that $C(t)$ undergoes changes that are accurately predicted by critical thresholds T_j^{ANC} given in Eq. (4). That is, there are three regions $T \in [T_{j+1}^{ANC}, T_j^{ANC}]$, and ANC events occur at approximately the same rate within each region. (C) A Pearson correlation coefficient ρ quantifies the extent to which STM cascades predominantly follow along the manifold via WFP. It is computed by comparing pairwise-distances $d_{ii'} \in \mathbb{R}^2$ between vertices v_i to $v_{i'}$ in the original 2D ambient space in which the ring manifold lies to pairwise-distances $\hat{d}_{ii'} \in \mathbb{R}^N$ between a nonlinear embedding of N vertices via STM Cascade Maps (see Methods Section ‘Simplicial cascade maps’), wherein a distance reflects the time required for a cascade to travel between vertices. (D)–(F) Similar information as in (A)–(C), but for the C. Elegans neuronal complex.

T was guided by the bifurcation diagrams in Fig. 5(A). We chose these particular values to highlight the impact of Δ and T on WFP and ANC properties. In particular, cascades exhibiting WFP and no ANC will have linear growth for $q(t)$ and the number of clusters $C(t)$ does not increase. (Note that it would be quadratic growth for WFP on the 2D manifold shown in Fig. 1, cubic growth for 3D manifolds, and so on.) On the other hand, cascades exhibiting WFP and ANC will have very rapid growth for $q(t)$ and an initial spike for the number of clusters $C(t)$. $C(t)$ can later decrease as clusters merge together. Finally, cascades do not spread if they neither exhibit WFP nor ANC.

Observe in Figs. 5(B) and 5(C) that these qualitative features occur for different choices of T and Δ exactly as predicted by our bifurcation theory. First, there is no spreading when $T = 0.5$ and $\Delta \in \{0.1, 0.5\}$ (left and center columns), or when $T \in \{0.35, 0.5\}$ and $\Delta = 0.9$ (right column), since $T > T_0^{WFP}$ and $T > T_0^{ANC}$ in these cases and there is neither WFP nor ANC. Second, there is a sharp rise in the number of clusters and rapid, super-linear growth only when $T \in \{0.05, 0.1\}$ and $\Delta = 0.1$ (left column) and when $T = 0.05$ with $\Delta = 0.5$ (center column), since $T < T_0^{WFP}$ and $T < T_0^{ANC}$ in these cases and both WFP and ANC occur. Third, for all other values of T and Δ , the curves exhibit linear growth when t is small, since $T < T_0^{WFP}$ and $T > T_0^{ANC}$ and there is WFP but no ANC. (The growth rate of spreading can be faster at later times t , since our bifurcation theory focuses on the nature of spreading dynamics at early stages of the cascades.)

One can also observe that increasing either T or Δ generically slows the spread of STMs cascades, and in particular, it slows the rates of both WFP and ANC behaviors. This is predicted by the other critical thresholds given in Eqs. (3) and (4), which we plot in Fig. 6 for different values of $j \geq 0$. In Figs. 6(A), we use color to depict the average rate of change for $q(t)$ at time $t = 5$, which is an empirical measure for WFP speed. We predict linear growth for $q(t)$ at a rate of $\frac{dq}{dt} \approx 2j - 2$ for $T \in [T_{j+1}^{WFP}, T_j^{WFP}]$, which is very close to what we empirically observe. Observe that as Δ increases, the ranges associated with larger j broaden, whereas the ranges associated with smaller j narrow. This can be understood by examining the right-hand side of Eq. (3) and noting that the first term is linear, whereas the second term is combinatorial. Hence, as STM cascades are more strongly influenced by 2-simplex interactions, slower WFP becomes a more dominant phenomenon across the T -parameter space.

In Figs. 6(B), we use color to depict the average number of clusters $C(t)$ at time $t = 5$, which is an empirical measure for the rate of ANC. Our bifurcation theory predicts three ranges $T \in [T_{j+1}^{ANC}, T_j^{ANC}]$, and as expected, the observed number of clusters is similar within these ranges and different across them. Importantly, increasing Δ causes all of the thresholds T_j^{ANC} to

approach 0. Thus, for any fixed T , increasing Δ will cause ANC events to vanish altogether. So while thresholding and higher-order interactions play a similar mechanistic role in that they both suppress ANC and allow WFP, higher-order interactions achieve this much more effectively.

In Figs. 6(D) and 6(E), we depict similar information as Figs. 6(A) and 6(B), except it is computed for the *C. Elegans* neuronal complex, rather than a noisy ring complex for which the bifurcation theory was developed. See Methods Section ‘Critical Regimes for *C. Elegans*’ for further information. Despite being outside the assumptions of these equations, they do a reasonable job of predicting the qualitative behavior of WFP and ANC. Specifically, dynamical changes still occur near the bifurcation lines for STM cascades on the neuronal complex. These changes are not as abrupt as those shown in Figs. 6(A) and 6(B), since the neuronal complex has heterogeneous 1-simplex degrees, which is known to blur bifurcation [87]. Nevertheless, the theory accurately predicts the general trend for how increasing Δ suppresses ANC and promotes WFP.

G. Latent geometry of simplicial cascades quantifies WFP vs ANC

It was proposed in [87] to quantitatively study competition between WFP and ANC using techniques from high-dimensional data analysis, nonlinear dimension reduction, manifold learning, and topological data analysis. The approach relied on constructing ‘contagion maps’ in which a set of vertices \mathcal{C}_0 in a graph are nonlinearly embedded in a Euclidean metric space so that the distances between vertices reflect the time required for contagions to traverse between them. Contagion maps are similar to other nonlinear embeddings that are based on diffusion [26] and shortest-path distance [88], but in contrast, they provide insights about the dynamics of thresholded cascades (as opposed to the dynamics of heat diffusion, for example). We generalize this approach by attributing the vertices in a simplicial complex with a latent geometry so that pairwise distances between vertices reflect the time required for STM cascades to traverse between them. See Methods Section ‘Simplicial cascade maps’ for details on this construction. Each cascade map uses J different initial conditions with cluster seeding yield an embedding $\{v_i\} \mapsto \{\mathbf{z}^{(i)}\} \in \mathbb{R}^J$, and for each embedding we compute the Pearson correlation coefficient ρ between pairwise distances $\|\mathbf{z}^{(i)} - \mathbf{z}^{(j)}\|_2$ in the latent embedding and pairwise distances between vertices in the original ambient space.

In Figs. 6(C) and (F), we use the high-dimensional geometry of simplicial cascade maps to quantitatively study the competing phenomena for WFP and ANC for a noisy ring complex and the *C. Elegans* neuronal complex, respectively. We use color to visualize ρ for different simplicial cascade maps using STM cascades with different choices for Δ and T . Larger values of ρ indicate parameter choices in which cascades exhibit increased amount of WFP versus ANC, whereas smaller ρ indicate the opposite.

Observe for both simplicial complexes that there is a regime that exhibits larger ρ values, and that regime requires that T and Δ are neither too larger nor too small. In this regime, the geometry of simplicial cascade maps best matches the original 2D geometry, which occurs because the STM cascades predominantly exhibit WFP along the geometric manifold and are not disrupted by ANC across the long-range simplices (i.e., topological ‘noise’). By comparing the panels in Fig. 6(C) to those in Figs. 6(A) and 6(B), the regions of larger ρ coincide with regions with slow WFP and unlikely ANC, as predicted by our bifurcation theory. Finally, observe that the ρ values are generally larger for the noisy ring complex than for the *C. Elegans* complex. This occurs because our synthetic noisy ring complex has much less degree heterogeneity than the *C. Elegans* neuronal complex, which reduces the extent to which STM cascades can exhibit WFP and little-to-no ANC.

III. DISCUSSION

Nonlinear cascades arise in diverse types of social, biological, physical and technological systems, many of which are insufficiently represented by cascade models that restricted to pairwise (i.e., dyadic) interactions [23, 25, 29, 37, 46, 52, 62, 68, 73, 94]. Thus motivated, we have proposed a simplicial threshold model (STM) for cascades over simplicial complexes that encode dyadic, triadic, and higher-order interactions. Our model complements other higher-order generalization for epidemic modeling [1, 7, 24, 42, 45, 86, 89], social contagions [30, 67], and consensus [65, 66, 81, 95]. By assigning the states of active/inactive to individual vertices as well as groups of vertices, STM cascades provide a new modeling framework that can help bridge individual-focused models (e.g., social contagions and neuronon interactions) with group-focused models (e.g., group decision making and interacting cortical columns interactions). In particular, simplicial cascades allow for the modeling of ‘multidimensional cascades’ in which the states of individuals influence the states of groups, and vice versa, and such interactions cannot be appropriately represented by graph-based models. Herein, the states of higher-dimensional simplices are immediately determined by vertices’ states, and it would be interesting in future work to explore more complicated dependencies such as allowing time lags between when a vertex becomes active and when its adjacent higher-dimensional simplices subsequently become active.

By studying STM cascades over ‘noisy geometric complexes’—a family of spatially embedded simplicial complexes that contain both short- and long-range k -simplices—our work reveals the interplay between higher-order dynamical nonlinearity and the multidimensional geometry of simplicial complexes to be a promising direction for research into how complex systems

organize the spatio-temporal patterns of cascade dynamics. In particular, we have shown that the coordination of higher-order coupling and thresholding enables STM cascades to robustly suppress the appearance of new clusters (ANC), enabling local wavefront propagation (WFP) along a geometrical substrate. In other words, STM cascades can propagate along k -dimensional geometrical channels (i.e., a sequence of “lower adjacent” k -simplices) despite the presence of long-range simplices (which introduce a “topological noise” to the geometry). While [58, 87] presents bifurcation theory describing how thresholding impacts WFP and ANC on noisy geometric networks containing short- and long-range edges, no prior work has explored the effects of higher-order coupling on WFP and ANC. This is problematic, since understanding whether a cascade predominantly spreads locally or nonlocally significantly impacts the steps that one takes, e.g., to predict and control cascades [5, 27, 31–33, 41, 43, 44, 59, 63, 69, 74]. Our bifurcation theory for STM cascades over noisy ring complexes that lie on 1D manifolds (see Fig. 2 and Eqs. (3) and (4)) was shown to accurately predict how WFP and ANC change depending on parameters of the cascade (i.e., threshold T and a parameter Δ that tunes the relative strength of 2-simplex interactions) and parameters of the noisy geometric complex (i.e., the number of geometric edges $d^{(G)}$, and nongeometric edges, $d^{(NG)}$, per vertex, as well as the number of 2-simplices, d^2). This theory characterizes the absence/presence of WFP and ANC and their respective rates, and it provides a solid theoretical foundation to support the exploration of WFP and ANC for higher-order cascades in a variety applied settings (e.g., belief propagation, epidemic spreading, cascading failures, and so on).

Our work provides important insights for higher-order information processing in neuronal networks and other complex systems. Higher-order dependencies are widely observed for neuronal activity [77, 94], yet theory development for neuronal cascades is largely restricted to pairwise-interaction models [54]. Thus motivated, we studied STM cascades over a ‘neuronal complex’ that represents the structural and higher-order nonlinear dynamical dependencies among neurons in nematode *C. Elegans*. We have shown that thresholding and higher-order interactions can collectively orchestrate the spatio-temporal patterns of STM cascades that spread across the multidimensional geometry of a neuronal complex, which we predict to be an important mathematical mechanism that can help brains direct cascading neuronal cascades and optimize the expressiveness and efficiency of cascades’ spatio-temporal patterns (see Fig. 4). Given the importance of efficiency in brains, simplicial-complex modeling will likely provide new perspectives on other types of efficiency, such as wiring efficiency [14] (which must address the issue that higher-order interactions may possibly be structural and/or functional). It is also worth noting that we have proposed an intentionally simple model for higher-order cascades with the goal of gaining concrete, analytically tractable insights. Future work should investigate the combined effects of other dynamical properties of neurons (e.g., refractory periods, inhibition, and stochasticity [10]) and other dynamical behaviors such as local/nonlocal patterns for synchronized neuron firings (which may benefit from recent synchronization theory for higher-order systems [16, 17, 36, 70, 84]).

Finally, we have introduced a technique called ‘simplicial cascade maps’ that embed a simplicial complex in a latent metric space. This nonlinear embedding extends contagion maps [87], which are recovered under the assumption of 1D STM cascades, and both mappings embed vertices so that the distance between vertices reflects how long cascades take to traverse from one vertex to another. Simplicial cascade maps generalize the well-developed field of graph embedding to the context of simplicial complexes, and we have used them to quantitatively study the extent to which STM cascades follow geometrical channels within a simplicial complex, i.e., as opposed to exhibiting nonlocal ANC phenomena. Although it is not our focus herein, simplicial cascade maps are expected to support higher-order generalizations of methodology development for manifold learning, topological data analysis, and nonlinear dimension reduction. Notably, STM cascades can robustly follow geometrical substrate despite the presence of topological noise, which is a property that can benefit these data-science pursuits when they are applied to noisy data.

IV. METHODS

A. Data and code availability

A codebase that implements STM cascades over noisy geometric complexes and reproduces our computational experiments is available in a Python library [97]. Documentation on how to use this software is available at [98]. The *C. Elegans* synapse network with physical vertex positions is publicly available and was downloaded from [47, 85].

B. STM cascades

In the text above, we focused on the case of 2D STM cascades. We now define a general version for STM cascades of dimension $\kappa \geq 1$. At time step $t + 1$, the state $x_i^0(t)$ of each vertex v_i possibly changes according to the threshold criterion given by Eq. (2)

except that we now define the simplicial exposure to be

$$R_i^t = \sum_{k=1}^{\kappa} \alpha_k f_i^k(t), \quad (5)$$

where $f_i^k(t) = \frac{1}{d_i^k} \sum_{j \in \mathcal{N}_A^k(i)} x_j^k(t)$ is the fraction of vertex v_i 's neighboring k -simplices that are active and $\{\alpha_k\}$ are nonnegative weights that satisfy $1 = \sum_k \alpha_k$. The choice $\alpha_1 = (1 - \Delta)$, $\alpha_2 = \Delta$ and $\kappa = 2$ recovers the model for 2D STM cascades that we studied above.

C. Cluster seeding

We initialize an STM cascade at a vertex v_i with *cluster seeding*, which we define as follows. Let $\mathcal{N}^1(i) \subset \mathcal{C}_0$ denote the set of vertices that are adjacent to v_i through 1-simplices. We set $x_j^0(0) = 1$ for any $j \in \mathcal{N}^1(i)$ at time $t = 0$ and $x_{j'}^0(0) = 0$ for any $j' \notin \mathcal{N}^1(i)$. Thus, the size of an STM cascade at time $t = 0$ is $q(0) = d_i^1$, which can possibly vary depending on the vertex degrees. Note that the seed vertex v_i itself is not in the set $\mathcal{N}^1(i)$, since we assume no self loops. Therefore $x_i^0(0)$ is inactive at $t = 0$, but it will very likely become active at time $t = 1$ (excluding the situation of pathologically large Δ and T).

D. Generative model for noisy ring complexes

We construct noisy ring complexes by considering the clique complexes associated with noisy ring lattices [87]. First, we place N vertices v_i at angles $\theta_i = 2\pi(i/N)$ for $i \in \{1, \dots, N\}$. We then add geometric edges by connecting each vertex to its $d^{(G)}$ nearest neighbors. We assume $d^{(G)}$ to be an even number so that $d^{(G)}/2$ edges go in either direction along the 1D manifold. Next, we add non-geometric edges uniformly at random between the vertices so that each vertex has exactly $d^{(NG)}$ non-geometric edges. We add non-geometric edges using the configuration model, except we add a re-sampling procedure to avoid adding an edge that already exists as a geometric edge. The resulting graph is a noisy ring lattice, and we study its associated clique complex, which we define as a *noisy ring complex*. (Recall that a *clique complex* is a simplicial complex that is derived from a graph, and there is a one-to-one correspondence between each clique involving $(k + 1)$ vertices in the graph and each k -simplex in the simplicial complex.) Finally, each k -simplex is then defined to be geometric or non-geometric, depending on whether it involves one or more non-geometric edge.

This generative model yields noisy ring complexes that are specified by three parameters: N , $d^{(G)}$ and $d^{(NG)}$. We also define the ratio $\alpha = d^{(NG)}/d^{(G)}$ of non-geometric to geometric degrees.

Noisy ring complexes are particularly amenable to theory development because they promote degree regularity. Specifically, they are *1-simplex degree regular* in that each vertex v_i is adjacent to exactly $d_i^1 = d^{(G)} + d^{(NG)}$ 1-simplices, where $d^{(G)}$ and $d^{(NG)}$ are the geometric and non-geometric 1-simplex degrees, respectively. The degrees d_i^k of higher-order simplices are not degree regular; however, the geometric degrees $d_i^{k,G}$ for $k \geq 1$ are identical across vertices due to the symmetry of the geometric substrate (i.e., the ‘sub’ simplicial complex that includes only geometric simplices).

While STM cascades can be studied over any simplicial complex, we focus herein on clique complexes, which helps facilitate the identification of adjacencies among k -simplices. If \mathbf{A} is the graph’s adjacency matrix so that $A_{ij} = 1$ if $(v_i, v_j) \in \mathcal{C}_1$ and $A_{ij} = 0$ otherwise, then an entry B_{ij} in matrix $\mathbf{B} = \mathbf{A}^2 * \mathbf{A}$ encodes the number of 2-simplices that are shared by vertices v_i and v_j . (Here, $*$ denotes the Hadamard, or ‘entrywise’, product.) In this work, we make use of matrices \mathbf{A} and \mathbf{B} when numerically implementing 2D STM cascades over clique complexes.

E. Entropy calculation

We use Shannon entropy in Fig. 4(C) to quantify the diversity of spatio-temporal patterns of 2D STM cascades on a C. Elegans neuronal complex, and we compute it as follows. In each panel of Fig. 4(A), we plot (top) cascade size $q(t)$ and (bottom) the number of spatially distant cascade clusters $C(t)$, and different curves indicate $q(t)$ and $C(t)$ for different initial conditions with cluster seeding. Focusing on $t = 5$, we consider the sets $\{q(5)\}$ and $\{C(5)\}$ and approximate their probability distributions by constructing histograms with 20 bins. Letting p_i denote the fraction of entries that fall into the i -th bin, we compute the associated discrete Shannon entropy

$$h = - \sum_{i=1}^{20} p_i \log p_i. \quad (6)$$

We note that our choice for the number of bins does effect the total entropy; however, we find that it has little effect on the qualitative behavior for how heterogeneity changes across the (T, Δ) parameter space, which is our main interest for Fig. 4(C).

F. Combinatorial analysis for bifurcation theory

We now present the derivation of our bifurcation theory given in Eqs. (3) and (4) for 2D STM cascades over noisy ring complexes. Recall for this model that N nodes are positioned along a the unit circle and are spaced apart by an angle $\delta = 2\pi/N$. Therefore, neighboring vertices are positioned apart by angles 1δ , 2δ , and so on. Also, recall that each vertex has exactly $d^{(G)}$ geometric edges to nearest-neighbor vertices and $d^{(NG)}$ non-geometric edges to other vertices, which are added uniformly at random. This generative model for noisy geometric complexes helps us to develop theory for ANC and WFP, but as we shall show, it also has important implications for such phenomena.

We first describe ANC in the limit of large N when the cascade size $q(t)$ is small. By definition, an ANC event occurs when a cascade propagates to a vertex v_i that is far from a cascade cluster, implying that all of its geometric k -simplices are inactive. It follows that the fractions of active adjacent k -simplices can only take on the following values

$$f_i^k \in \left\{ 0, \frac{1}{d_i^k}, \frac{2}{d_i^k}, \dots, \frac{d_i^{k,NG}}{d_i^k} \right\}, \quad (7)$$

depending on the number of active non-geometric k -simplices. For STM cascades over noisy ring complexes that are generated via the model that we describe in Methods Section ‘Generative model for noisy ring complexes’, we find that ANC events occur predominantly due to influences by non-geometric 1-simplices. In contrast, we find non-geometric 2-simplices to have a negligible effect on ANC in the limit of large N , small $q(t)$, and fixed $d^{(G)}$ and $d^{(NG)}$, which implies $f_i^2 \approx 0$ under these assumptions. Specifically, non-geometric 2-simplices (and higher-dimensional simplices) are rare, because non-geometric edges are added uniformly at random. Consider a vertex v_i that is distant from a cascade cluster, and suppose that it has one non-geometric edge to an active vertex v_j . That edge is the face of a 2-simplex only if v_i has a second non-geometric edge to a third vertex that is already adjacent to v_j . This occurs with probability $1 - [(N - 1 - d_i^1)/N]^{(d^{(NG)} - 1)} \sim \mathcal{O}(N^{-1})$, which approaches zero with increasing N . This result uses that there are $N - 1 - d_i^1$ possible vertices that v_i can connect to without creating a non-geometric 2-simplex v_j . Since non-geometric edges are created uniformly at random, each of the remaining non-geometric edges for v_i don’t create a 2-simplex with probability $[(N - 1 - d_i^1)/N]$. Moreover, $[(N - 1 - d_i^1)/N]^{(d^{(NG)} - 1)}$ gives the probability that none of them do. Subtracting this probability by 1 gives the probability that there is at least one non-geometric 2-simplex between v_i and v_j (that is, given that they are already connected by a non-geometric edge). Therefore, while non-geometric 2-simplices (and higher-dimensional simplices) do arise in our generative model for noisy ring complexes, they are rare and have little effect on ANC for large systems.

To obtain the critical thresholds given in Eq. (4), we approximate $R_i(t) \approx (1 - \Delta) f_i^1$ and observe that

$$f_i^1 \in \left\{ 0, \frac{1}{d^{(G)} + d^{(NG)}}, \dots, \frac{d^{(NG)}}{d^{(G)} + d^{(NG)}} \right\}, \quad (8)$$

which uses that the 1-simplices are degree regular. If one considers a variable threshold T , then the probability that ANC events occur will significantly change as T surpasses the different $R_i(t)$ values corresponding to different f_i^1 . For example, there are no ANC events when $T > (1 - \Delta) \frac{d^{(NG)}}{d^{(G)} + d^{(NG)}}$.

Notably, our bifurcation theory for ANC naturally extends to κ -dimensional STM cascades in which $R_i(t) = \sum_{k=1}^{\kappa} \alpha_k f_i^k(t)$. In this case, non-geometric k -simplices with $k > 1$ also have little effect on ANC, and the critical thresholds are identical to those in Eq. (4) with the variable substitution $(1 - \Delta) \mapsto \alpha_1$.

We next develop bifurcation theory for WFP dynamics, and in this case, higher-dimensional simplices have a significant effect. Our analysis stems from considering boundary vertices that are not yet active but have geometric simplicial neighbors—i.e., adjacent geometric 1-simplices, geometric 2-simplices, etc.—that are active. The propagation speed of a wavefront along a geometric channel is determined by the number of boundary vertices that become active upon each time step. For example, in Fig. 7(A) we visualize a noisy ring complex with $d^{(G)} = 6$ so that there are $d^{(G)}/2 = 3$ boundary vertices $\{v_1, v_2, v_3\}$ for the clockwise-progressing wavefront. (Recall that each vertex connects to $d^{(G)}/2$ nearest-neighbor vertices in either direction along the ring manifold.) Therefore, the speed of a wavefront is either 1, 2, or 3, depending on how many of them become active at each time step. Note that the cascade exposure $R_i(t)$ defined in Eq. (2) will be different for each boundary vertex, and because they are enumerated closest-to-farthest from the wavefront, one has $f_1^k(t) \geq f_2^k(t) \geq f_3^k(t)$ and $R_1(t) \geq R_2(t) \geq R_3(t)$. Therefore, as a threshold T_i increases, the criterion $R_i(t) > T_i$ defined in Eq. (1) will first fail for v_3 , then v_2 , and finally v_1 . The wavefront shown in Fig. 7 won’t propagate for any threshold that is larger than $R_1(t)$.

The $R_i(t)$ values of boundary vertices reveal critical threshold values for WFP, and we identify them for noisy ring complexes

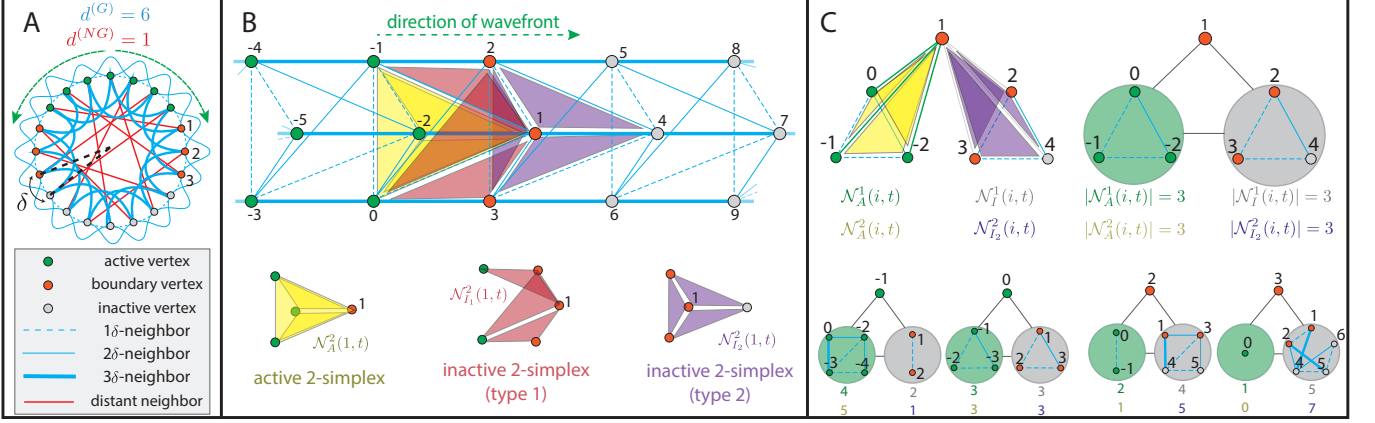


FIG. 7. **Bifurcation theory obtained by examining the connections between boundary vertices and active/inactive 1- and 2-simplices.** **A.** Visualization of a noisy ring complex with $d^{(G)} = 6$ and $d^{(NG)} = 1$ with N vertices that are spaced apart by an angle $\delta = 2\pi/N$. Linestyles highlight that edges connect neighbors with different proximity, and we label vertices so that vertex v_1 is positioned 1δ to the right of the wavefront, v_2 is at position 2δ , and so on. The speed of WFP is determined by the number of boundary vertices $\{v_1, v_2, v_3\}$ that become active upon the next time step. **B.** Visualization of active and inactive k -simplices for the boundary vertex v_1 that is closest to the wavefront. For each v_i , we define a set $\mathcal{N}_A^k(i, t)$ of adjacent k -simplices that are active and sets $\mathcal{N}_{I_1}^k(i, t)$ and $\mathcal{N}_{I_2}^k(i, t)$ of inactive 2-simplices that are type 1 and 2, respectively. (Recall Fig. 2.) **C.** By identifying a set of neighboring active vertices (green shaded regions) for a boundary vertex v_i , one can compute the number of adjacent 1- and 2-simplices that are active by counting the number of those vertices and the number of edges among them, respectively. One can identify the number of inactive 1-simplices and type-2 inactive 2-simplices in a similar way (gray shaded regions). This approach is depicted for vertex v_1 (top) as well as other nearby vertices (bottom), and the associated numbers are indicated for each.

by considering how each v_i is adjacent to geometric k -simplices that are either active or inactive. We may assume that the non-geometric k -simplices are inactive in the limit of large N and small cascades size $q(t)$ [technically, a non-geometric k -simplex is active with probability that is at most $\mathcal{O}(q(t)/N)$], and so we initially focus on $d^{(NG)} = 0$. We will later allow for nonzero $d^{(NG)}$ when we compute the fractions $f_i^k(t)$. To this end, we define for each v_i the sets $\mathcal{N}^k(i)$ of adjacent k -simplices, which we partition into sets $\mathcal{N}_A^k(i, t)$ and $\mathcal{N}_I^k(i, t)$ of adjacent k -simplices that are active and inactive, respectively, at time t . Note that $\mathcal{N}^k(i) = \mathcal{N}_A^k(i, t) \cup \mathcal{N}_I^k(i, t)$ and $d_i^k = |\mathcal{N}^k(i)|$ is the degree of v_i with respect to k -simplices. With these definitions, the fractions of active k -simplices are given by

$$f_i^k(t) = \frac{|\mathcal{N}_A^k(i, t)|}{d_i^k}. \quad (9)$$

In Fig. 7(B), we visualize a wavefront propagating along a geometric channel for the noisy ring complex shown in Fig. 7(A). Vertices are positioned so that we may more easily identify whether 2-simplices are active or inactive. Focusing on the boundary vertex v_1 that is closest to the wavefront and has the largest exposure $R_i(t)$, we illustrate its set of adjacent 2-simplices that are active. Because v_1 is adjacent to $|\mathcal{N}_A^1(1, t)| = 3$ active 1-simplices and $|\mathcal{N}_A^2(1, t)| = 3$ active 2-simplices, it follows that $f_1^1(t) = \frac{3}{d_1^1}$ and $f_1^2(t) = \frac{3}{d_1^2}$. (Note that the denominators include both geometric and non-geometric k -simplices.) We also visualize in Fig. 7(B) the inactive 2-simplices that are adjacent to boundary vertex v_1 . Recall from Fig. 2 that there are two types of inactive 2-simplices, depending on whether a 2-simplex contains only one active vertex (type 1) or no active vertices (type 2). We let $\mathcal{N}_{I_1}^2(i, t)$ and $\mathcal{N}_{I_2}^2(i, t)$ denote the sets of inactive 2-simplices of types 1 and 2, respectively, and depict them for v_1 . Observe that $|\mathcal{N}_I^1(1, t)| = |\mathcal{N}_{I_1}^2(1, t)| = |\mathcal{N}_{I_2}^2(1, t)| = 3$.

In Fig. 7(C), we highlight that one can easily compute the number of active 1- and 2-simplices that are adjacent to a boundary vertex v_i using three steps. First, we identify the set $\{v_j | (i, j) \in \mathcal{N}_A^1(i, t)\}$ of active vertices that are connected to v_i by active 1-simplices (see green shaded regions). Second, we count the number of vertices in that set, which yields $|\mathcal{N}_A^1(i, t)|$ since there is a one-to-one correspondence between these vertices and the active 1-simplices that are adjacent to v_i . Third, we count the number of edges among those vertices, which yields $|\mathcal{N}_A^2(i, t)|$ since there is a one-to-one correspondence between those edges and active 2-simplices. We can also calculate the number of type-2 inactive 2-simplices in a similar way. That is, we first identify the set $\{v_j | (i, j) \in \mathcal{N}_I^1(i, t)\}$ of inactive vertices that are connected to v_i by inactive 1-simplices (see gray shaded regions in Fig. 7(C)). We then count how many vertices are in the set (which yields $|\mathcal{N}_I^1(i, t)|$) and the number of edges among those vertices (which yields $|\mathcal{N}_I^2(i, t)|$). The upper part of Fig. 7(C) illustrates this approach for v_1 , and we do not visualize type-1 inactive 2-simplices, because they are more difficult to compute directly but can be found after the other sets are determined: $|\mathcal{N}_{I_1}^2(i, t)| = d_i^2 - |\mathcal{N}_A^2(i, t)| - |\mathcal{N}_{I_2}^2(i, t)|$. The lower part of Fig. 7(C) illustrates this approach for the other two boundary

vertices $\{v_2, v_3\}$ as well as two vertices $\{v_{-1}, v_0\}$ that are already active, since they are to the left of the wavefront.

Importantly, because each vertex has exactly $d^{(G)}/2$ 1-simplices going in either side along the ring manifold left, there is always a clique of edges among vertices in a set $\{v_j | (i, j) \in \mathcal{N}_A^1(i, t)\}$ for the boundary vertices. (This is not true for active vertices, such as v_{-1} , as shown in the lower part of Fig. 7(C).) Therefore, if a boundary vertex has s_j active 1-simplices, then it must also have $\binom{s_j}{2}$ active 2-simplices. It follows that the different possible f_i^1 values for a boundary vertex v_i are given by

$$f_i^1 \in \left\{ 0, \frac{1}{d_i^1}, \frac{2}{d_i^1}, \dots, \frac{d^{(G)/2}}{d_i^1} \right\}, \quad (10)$$

and the corresponding f_i^2 values are

$$f_i^2 \in \left\{ 0, \frac{1}{d_i^2} \binom{1}{2}, \frac{1}{d_i^2} \binom{2}{2}, \dots, \frac{1}{d_i^2} \binom{d^{(G)/2}}{2} \right\}. \quad (11)$$

We enumerate these possibilities by j and use the definition $R_i(t) = (1 - \Delta)f_i^1 + \Delta f_i^2$ to obtain the critical threshold values for WFP given by Eq. (3). Notably, whenever $T \in [T_{j+1}^{WFP}, T_j^{WFP})$, $(j+1)$ boundary vertices will become active upon each time step. Since wavefronts progress both clockwise and counter-clockwise around the ring manifold, the cascade size $q(t)$ will grow at a rate $2j + 2$.

More generally, we derive a generalized set of bifurcation lines that describe WFP for κ -dimensional STM cascades:

$$T_j^{WFP} = \sum_{k=1}^{\kappa} \alpha_k \frac{1}{d_i^2} \binom{s_j^{(G)}}{k}. \quad (12)$$

G. Critical regimes for *C. Elegans*

Since the theory assumes degree regularity, but the empirical neuronal complex is degree heterogeneous we use the median geometric degree, non-geometric degree, and triangular degree across vertices, $d^{(G)} = 8$, $d^{(NG)} = 2$, and $d^2 = \sum_{i,j} B_{ij} = 34$ to evaluate the critical threshold regimes, respectively. We run the simplicial threshold model cascades on the undirected *C. Elegans* synapse network since our theory doesn't involve directed k -simplices although it can be carefully extended to the directed case.

H. Simplicial cascade maps

We introduce a notion of latent geometry for simplicial-complexes called *simplicial cascade maps* in which the set $\mathcal{C}_0 = \{1, \dots, N\}$ of vertices is nonlinearly mapped as a set of points (i.e., a ‘point cloud’) in an J -dimensional Euclidean metric space \mathbb{R}^J . Simplicial cascade maps directly generalize contagion maps [87], which are recovered under the choice of 1D STM cascades (and which do not utilize k -simplices for $k > 1$).

We construct simplicial cascade maps using the activation times for STM cascades. Given J realizations of a STM cascade on a simplicial complex with different initial conditions with cluster seeding, the associated STM map is a map $\{v_i\} \mapsto \{\boldsymbol{\tau}^{(i)}\} \in \mathbb{R}^J$ in which each vertex $v_i \in \mathcal{C}_0$ maps to a point $\boldsymbol{\tau}^{(i)} = [\tau_1^{(i)}, \dots, \tau_J^{(i)}]^T$, where $\tau_j^{(i)}$ is the activation time for vertex v_i for the STM cascade with the j -th initial condition.

In practice, we often let $J = N$ so that the j -th initial condition corresponds to seed clustering at vertex v_j . However, extra attention is required for handling cascades that don't saturate the network, in which case there would be $\tau_j^{(i)}$ values that are undefined. Herein, we choose to neglect such cascades. See [87] for alternative strategies that were developed under similar circumstances for contagion maps.

[1] Alain Barrat, Guilherme Ferraz de Arruda, Iacopo Iacopini, and Yamir Moreno. Social contagion on higher-order structures. *arXiv:2103.03709*.

[2] Marc Barthélémy. Spatial networks. *Physics Reports*, 499(1-3):1–101, 2011.

[3] Danielle Smith Bassett and ED Bullmore. Small-world brain networks. *The Neuroscientist*, 12(6):512–523, 2006.

[4] Plenz D, Beggs JM. Neuronal avalanches in neocortical circuits. *Journal of Neuroscience*, 23(35):11167–1117, 2003.

[5] Kara Bentley, Charlene Chu, Cristina Nistor, Ekin Pehlivan, and Taylan Yalcin. Social media engagement for global influencers. *Journal of Global Marketing*, pages 1–15, 2021.

- [6] Hlinka J, Keilholz S, Petri G, Billings J, Saggar M. Simplicial and topological descriptions of human brain dynamics. *Network Neuroscience*, 5(2):549–568, 2021.
- [7] Ágnes Bodó, Gyula Y Katona, and Péter L Simon. SIS epidemic propagation on hypergraphs. *Bulletin of Mathematical Biology*, 78(4):713–735, 2016.
- [8] Marian Boguna, Ivan Bonamassa, Manlio De Domenico, Shlomo Havlin, Dmitri Krioukov, and M Ángeles Serrano. Network geometry. *Nature Reviews Physics*, 3(2):114–135, 2021.
- [9] Désiré Bollé, Rob Heylen, and NS Skantzos. Thermodynamics of spin systems on small-world hypergraphs. *Physical Review E*, 74(5):056111, 2006.
- [10] Romain Brette, Michelle Rudolph, Ted Carnevale, Michael Hines, David Beeman, James M Bower, Markus Diesmann, Abigail Morrison, Philip H Goodman, Frederick C Harris, et al. Simulation of networks of spiking neurons: a review of tools and strategies. *Journal of Computational Neuroscience*, 23(3):349–398, 2007.
- [11] Dirk Brockmann and Dirk Helbing. The hidden geometry of complex, network-driven contagion phenomena. *Science*, 342(6164):1337–1342, 2013.
- [12] Charles D. Brummitt, Raissa M. D’Souza, and E. A. Leicht. Suppressing cascades of load in interdependent networks. *Proceedings of the National Academy of Sciences*, 109(12):E680–E689, 2012.
- [13] Paul G. et al. Buldyrev S., Parshani R. Catastrophic cascade of failures in interdependent networks. *Nature*, 464:1025–1028, 2010.
- [14] Sporns O, Bullmore, E. The economy of brain network organization. *Nature Review Neuroscience*, 13:336–349, 2012.
- [15] Ghanbarnejad F. et al. Cai W., Chen L. Avalanche outbreaks emerging in cooperative contagions. *Nature Physics*, 11,:936–940, 2015.
- [16] Lucille Calmon, Juan G Restrepo, Joaquín J Torres, and Ginestra Bianconi. Topological synchronization: explosive transition and rhythmic phase. *arXiv preprint arXiv:2107.05107*, 2021.
- [17] Xu Can, Wang Xuebin, and Skardal Per Sebastian. Bifurcation analysis and structural stability of simplicial oscillator populations. *Physical Review Research*, 2:023281, Jun 2020.
- [18] Timoteo Carletti, Federico Battiston, Giulia Cencetti, and Duccio Fanelli. Random walks on hypergraphs. *Physical Review E*, 101:022308, Feb 2020.
- [19] Timoteo Carletti, Duccio Fanelli, and Renaud Lambiotte. Random walks and community detection in hypergraphs. *Journal of Physics: Complexity*, 2(1):015011, 2021.
- [20] Damon Centola. The spread of behavior in an online social network experiment. *Science*, 329(5996):1194–1197, 2010.
- [21] Damon Centola, Víctor M Eguíluz, and Michael W Macy. Cascade dynamics of complex propagation. *Physica A: Statistical Mechanics and its Applications*, 374(1):449–456, 2007.
- [22] Damon Centola and Michael Macy. Complex contagions and the weakness of long ties. *American Journal of Sociology*, 113(3):702–734, 2007.
- [23] MacLean JN Chambers B. Higher-order synaptic interactions coordinate dynamics in recurrent networks. *PLoS Computational Biology*, 12(8):e1005078., 2016.
- [24] Sandeep Chowdhary, Aanjaneya Kumar, Giulia Cencetti, Iacopo Iacopini, and Federico Battiston. Simplicial contagion in temporal higher-order networks. *arXiv:2105.04455*.
- [25] Andrea Civilini, Nejat Anbarci, and Vito Latora. Evolutionary game model of risk propensity in group decision making. *arXiv preprint arXiv:2104.11270*, 2021.
- [26] Ronald R Coifman and Stéphane Lafon. Diffusion maps. *Applied and Computational Harmonic Analysis*, 21(1):5–30, 2006.
- [27] Vittoria Colizza, Alain Barrat, Marc Barthelemy, Alain-Jacques Valleron, and Alessandro Vespignani. Modeling the worldwide spread of pandemic influenza: baseline case and containment interventions. *PLoS Medicine*, 4(1):e13, 2007.
- [28] Vittoria Colizza, Alain Barrat, Marc Barthélemy, and Alessandro Vespignani. The role of the airline transportation network in the prediction and predictability of global epidemics. *Proceedings of the National Academy of Sciences*, 103(7):2015–2020, 2006.
- [29] Mayukh Dass and Gavin L Fox. A holistic network model for supply chain analysis. *International Journal of Production Economics*, 131(2):587–594, 2011.
- [30] de Arruda Guilherme Ferraz, Petri Giovanni, and Moreno Yamir. Social contagion models on hypergraphs. *Physical Review Research*, 2:023032, Apr 2020.
- [31] Ian Dobson, Benjamin A Carreras, Vickie E Lynch, and David E Newman. Complex systems analysis of series of blackouts: Cascading failure, critical points, and self-organization. *Chaos: An Interdisciplinary Journal of Nonlinear Science*, 17(2):026103, 2007.
- [32] Alexandre Dolgui, Dmitry Ivanov, and Boris Sokolov. Ripple effect in the supply chain: an analysis and recent literature. *International Journal of Production Research*, 56(1-2):414–430, 2018.
- [33] Joshua M Epstein, D Michael Goedecke, Feng Yu, Robert J Morris, Diane K Wagener, and Georgiy V Bobashev. Controlling pandemic flu: the value of international air travel restrictions. *PloS ONE*, 2(5):e401, 2007.
- [34] Ernesto Estrada, Jean-Charles Delvenne, Naomichi Hatano, José L Mateos, Ralf Metzler, Alejandro P Riascos, and Michael T Schaub. Random multi-hopper model: super-fast random walks on graphs. *Journal of Complex Networks*, 6(3):382–403, 2018.
- [35] Tizzani M, Ferraz de Arruda G. and Y. Moreno. Phase transitions and stability of dynamical processes on hypergraphs. *Communications Physics*, 4:24, 2021.
- [36] Gallo L. et al. Gambuzza L.V., Di Patti F. Stability of synchronization in simplicial complexes. *Nature Communications*, 12:1255, 2021.
- [37] Abdorasoul Ghasemi and Holger Kantz. Data-driven interaction analysis of line failure cascading in power grid networks. *arXiv preprint arXiv:2112.01061*, 2021.
- [38] Chad Giusti, Robert Ghrist, and Danielle S Bassett. Two’s company, three (or more) is a simplex. *Journal of computational neuroscience*, 41(1):1–14, 2016.
- [39] James P Gleeson. Binary-state dynamics on complex networks: Pair approximation and beyond. *Physical Review X*, 3(2):021004, 2013.
- [40] James P Gleeson and Diarmuid J Cahalane. Seed size strongly affects cascades on random networks. *Physical Review E*, 75(5):056103, 2007.

[41] Shi Gu, Fabio Pasqualetti, Matthew Cieslak, Qawi K Telesford, B Yu Alfred, Ari E Kahn, John D Medaglia, Jean M Vettel, Michael B Miller, Scott T Grafton, et al. Controllability of structural brain networks. *Nature Communications*, 6(1):1–10, 2015.

[42] Desmond John Higham and Henry-Louis de Kerorlay. Epidemics on hypergraphs: Spectral thresholds for extinction. *arXiv preprint arXiv:2103.07319*, 2021.

[43] Paul DH Hines, Ian Dobson, and Pooya Rezaei. Cascading power outages propagate locally in an influence graph that is not the actual grid topology. *IEEE Transactions on Power Systems*, 32(2):958–967, 2016.

[44] T Déirdre Hollingsworth, Neil M Ferguson, and Roy M Anderson. Will travel restrictions control the international spread of pandemic influenza? *Nature Medicine*, 12(5):497–499, 2006.

[45] Barrat A, et al. Iacobini I, Petri G. Simplicial models of social contagion. *Nature Communications*, 10:2485, 2019.

[46] Ryan G James, Nix Barnett, and James P Crutchfield. Information flows? a critique of transfer entropies. *Physical Review Letters*, 116(23):238701, 2016.

[47] Marcus Kaiser. C. elegans global network of 277 neurons. <https://www.dynamic-connectome.org/resources/>.

[48] Marcus Kaiser and Claus C. Hilgetag. Nonoptimal component placement, but short processing paths, due to long-distance projections in neural systems. *PLoS Computational Biology*, 2(7):e95, 2006.

[49] Werner M Kistler, Wulfram Gerstner, and J Leo van Hemmen. Reduction of the hodgkin-huxley equations to a single-variable threshold model. *Neural Computation*, 9(5):1015–1045, 1997.

[50] Steffen Klamt, Utz-Uwe Haus, and Fabian Theis. Hypergraphs and cellular networks. *PLoS Computational Biology*, 5(5):e1000385, 2009.

[51] Dmitri Krioukov, Fragkiskos Papadopoulos, Maksim Kitsak, Amin Vahdat, and Marián Boguná. Hyperbolic geometry of complex networks. *Physical Review E*, 82(3):036106, 2010.

[52] Nicolas Lanchier and Jared Neufer. Stochastic dynamics on hypergraphs and the spatial majority rule model. *Journal of Statistical Physics*, 151(1):21–45, 2013.

[53] Nicholas W Landry and Juan G Restrepo. Hypergraph dynamics: assortativity and the expansion eigenvalue. *arXiv preprint arXiv:2109.01099*, 2021.

[54] Daniel B Larremore, Woodrow L Shew, and Juan G Restrepo. Predicting criticality and dynamic range in complex networks: effects of topology. *Physical Review Letters*, 106(5):058101, 2011.

[55] Daqing Li, Bowen Fu, Yunpeng Wang, Guangquan Lu, Yehiel Berezin, H. Eugene Stanley, and Shlomo Havlin. Percolation transition in dynamical traffic network with evolving critical bottlenecks. *Proceedings of the National Academy of Sciences*, 112(3):669–672, 2015.

[56] Jingwen Li, Patrick A Kells, Ayla C Osgood, Shree Hari Gautam, and Woodrow L Shew. Collapse of complexity of brain and body activity due to excessive inhibition and mecp2 disruption. *Proceedings of the National Academy of Sciences*, 118(43), 2021.

[57] McNaughton B, Luczak A, and K. Harris. Packet-based communication in the cortex. *Nature Review Neuroscience*, 16:745–755, 2015.

[58] Barbara I Mahler. Analysis of contagion maps on a class of networks that are spatially embedded in a torus. *SIAM Journal on Applied Mathematics*, 81(4):1416–1440, 2021.

[59] Sonia Irshad Mari, Young Hae Lee, Muhammad Saad Memon, Young Soo Park, and Minsun Kim. Adaptivity of complex network topologies for designing resilient supply chain networks. *International Journal of Industrial Engineering*, 22(1), 2015.

[60] Seth A Marvel, Travis Martin, Charles R Doering, David Lusseau, and Mark EJ Newman. The small-world effect is a modern phenomenon. *arXiv preprint arXiv:1310.2636*, 2013.

[61] Naoki Masuda and Petter Holme. Predicting and controlling infectious disease epidemics using temporal networks. *F1000Prime Reports*, 5, 2013.

[62] Stouffer D, Mayfield, M. Higher-order interactions capture unexplained complexity in diverse communities. *Nature Ecology and Evolution*, 0062, 2017.

[63] John D Medaglia, Brian Erickson, Jared Zimmerman, and Apoorva Kelkar. Personalizing neuromodulation. *International Journal of Psychophysiology*, 154:101–110, 2020.

[64] Sayan Mukherjee and John Steenbergen. Random walks on simplicial complexes and harmonics. *Random Structures & Algorithms*, 49(2):379–405, 2016.

[65] Leonie Neuhäuser, Renaud Lambiotte, and Michael T Schaub. Consensus dynamics on temporal hypergraphs. *arXiv preprint arXiv:2109.04985*, 2021.

[66] Leonie Neuhäuser, Andrew Mellor, and Renaud Lambiotte. Multibody interactions and nonlinear consensus dynamics on networked systems. *Physical Review E*, 101(3):032310, 2020.

[67] Leonie Neuhäuser, Michael T Schaub, Andrew Mellor, and Renaud Lambiotte. Opinion dynamics with multi-body interactions. In *International Conference on Network Games, Control and Optimization*, pages 261–271. Springer, 2021.

[68] James Noonan and Renaud Lambiotte. Dynamics of majority rule on hypergraphs. *arXiv preprint arXiv:2101.03632*, 2021.

[69] Jukka-Pekka Onnela and Felix Reed-Tsochas. Spontaneous emergence of social influence in online systems. *Proceedings of the National Academy of Sciences*, 107(43):18375–18380, 2010.

[70] Millán Ana P., Torres Joaquín J., and Bianconi Ginestra. Explosive higher-order kuramoto dynamics on simplicial complexes. *Physical Review Letters*, 124:218301, May 2020.

[71] Ori Parzanchevski and Ron Rosenthal. Simplicial complexes: spectrum, homology and random walks. *Random Structures & Algorithms*, 50(2):225–261, 2017.

[72] Romualdo Pastor-Satorras, Claudio Castellano, Piet Van Mieghem, and Alessandro Vespignani. Epidemic processes in complex networks. *Reviews of Modern Physics*, 87(3):925, 2015.

[73] Petri G, Patania, A, and F. Vaccarino. The shape of collaborations. *EPJ Data Science*, 6,18, 2017.

[74] Surya D Pathak, Jamison M Day, Anand Nair, William J Sawaya, and M Murat Kristal. Complexity and adaptivity in supply networks: Building supply network theory using a complex adaptive systems perspective. *Decision Sciences*, 38(4):547–580, 2007.

[75] Bethany Percha, Rhonda Dzakpasu, Michał Żochowski, and Jack Parent. Transition from local to global phase synchrony in small world

neural network and its possible implications for epilepsy. *Physical Review E*, 72(3):031909, 2005.

[76] Giovanni Petri, Paul Expert, Federico Turkheimer, Robin Carhart-Harris, David Nutt, Peter J Hellyer, and Francesco Vaccarino. Homological scaffolds of brain functional networks. *Journal of The Royal Society Interface*, 11(101):20140873, 2014.

[77] Michael W Reimann, Max Nolte, Martina Scolamiero, Katharine Turner, Rodrigo Perin, Giuseppe Chindemi, Paweł Dłotko, Ran Levi, Kathryn Hess, and Henry Markram. Cliques of neurons bound into cavities provide a missing link between structure and function. *Frontiers in Computational Neuroscience*, 11:48, 2017.

[78] Robert Rosenbaum, Matthew A Smith, Adam Kohn, Jonathan E Rubin, and Brent Doiron. The spatial structure of correlated neuronal variability. *Nature Neuroscience*, 20(1):107–114, 2017.

[79] Alex Roxin, Hermann Riecke, and Sara A Solla. Self-sustained activity in a small-world network of excitable neurons. *Physical Review Letters*, 92(19):198101, 2004.

[80] Zhongyuan Ruan, Gerardo Iniguez, Márton Karsai, and János Kertész. Kinetics of social contagion. *Physical Review Letters*, 115(21):218702, 2015.

[81] Rohit Sahasrabuddhe, Leonie Neuhäuser, and Renaud Lambiotte. Modelling non-linear consensus dynamics on hypergraphs. *Journal of Physics: Complexity*, 2(2):025006, 2021.

[82] Woodrow L Shew and Dietmar Plenz. The functional benefits of criticality in the cortex. *The Neuroscientist*, 19(1):88–100, 2013.

[83] Woodrow L Shew, Hongdian Yang, Shan Yu, Rajarshi Roy, and Dietmar Plenz. Information capacity and transmission are maximized in balanced cortical networks with neuronal avalanches. *Journal of Neuroscience*, 31(1):55–63, 2011.

[84] Per Sebastian Skardal, Lluís Arola-Fernández, Dane Taylor, and Alex Arenas. Higher-order interactions improve optimal collective dynamics on networks. *arXiv preprint arXiv:2108.08190*, 2021.

[85] Marcus Kaiser Sreedevi Varier. Neural development features: Spatio-temporal development of the *caenorhabditis elegans* neuronal network. *PLoS Computational Biology*, 1(7):e1001044, 2011.

[86] Matamalas Joan T., Gómez Sergio, and Arenas Alex. Abrupt phase transition of epidemic spreading in simplicial complexes. *Physical Review Research*, 2:012049, Feb 2020.

[87] Dane Taylor, Florian Klimm, Heather A Harrington, Miroslav Kramár, Konstantin Mischaikow, Mason A Porter, and Peter J Mucha. Topological data analysis of contagion maps for examining spreading processes on networks. *Nature Communications*, 6(1):1–11, 2015.

[88] Joshua B Tenenbaum, Vin De Silva, and John C Langford. A global geometric framework for nonlinear dimensionality reduction. *Science*, 290(5500):2319–2323, 2000.

[89] Landry Nicholas W. and Restrepo Juan G. The effect of heterogeneity on hypergraph contagion models. *Chaos: An Interdisciplinary Journal of Nonlinear Science*, 30(10):103117, 2020.

[90] Duncan J. Watts. A simple model of global cascades on random networks. *Proceedings of the National Academy of Sciences*, 99(9):5766–5771, 2002.

[91] Duncan J Watts and Steven H Strogatz. Collective dynamics of ‘small-world’ networks. *Nature*, 393(6684):440–442, 1998.

[92] Choe Y, McCormick BH, and Koh W. Network connectivity analysis on the temporally augmented *C. elegans* web: A pilot study. 30(921.9), 2004.

[93] Shan Yu, Debin Huang, Wolf Singer, and Danko Nikolić. A small world of neuronal synchrony. *Cerebral Cortex*, 18(12):2891–2901, 2008.

[94] Shan Yu, Hongdian Yang, Hiroyuki Nakahara, Gustavo S. Santos, Danko Nikolić, and Dietmar Plenz. Higher-order interactions characterized in cortical activity. *Journal of Neuroscience*, 31(48):17514–17526, 2011.

[95] Wenwu Yu, Guanrong Chen, Wei Ren, Jürgen Kurths, and Wei Xing Zheng. Distributed higher order consensus protocols in multiagent dynamical systems. *IEEE Transactions on Circuits and Systems I: Regular Papers*, 58(8):1924–1932, 2011.

[96] Cameron Ziegler, Per Sebastian Skardal, Haimonti Dutta, and Dane Taylor. Balanced Hodge Laplacians optimize consensus dynamics over simplicial complexes. *arXiv preprint arXiv:2112.01070*, 2021.

[97] Bengier Ülgen Kılıç. Github, neuronal cascades. https://github.com/ulgenklc/Neuronal_Cascades.

[98] Bengier Ülgen Kılıç. Read the docs, neuronal cascades. <https://neuronal-cascades.readthedocs.io/en/latest/index.html>.